This article has been accepted for publication in IEEE Journal of Selected Topics in Signal Processing. This is the author's version which has not been fully edited and content may change prior to final publication. Citation information: DOI 10.1109/JSTSP.2025.3590607

Accelerating Multiuser Beamforming with Full-Dimension One-Bit Chains

Lina Liu and Dongning Guo

***Abstract*—Massive multiple-input multiple-output (MIMO) systems are vital for achieving high spectral efficiencies at mid-band and millimeter wave frequencies. Conventional hybrid MIMO architectures, which use fewer digital chains than antennas, offer a balance between performance, cost, and energy consumption but often prolong channel estimation. This paper proposes a novel architecture that integrates a set of full-dimension digital chains with one-bit analog-to-digital converters (ADCs) to overcome these limitations and provide an alternative trade-off. By assigning one digital chain to each receive antenna, the proposed approach captures energy from all receive antennas and accelerates angle-of-arrival (AoA) estimation and beam computation. Likelihood-based AoA estimation methods are developed to optimize analog beamforming in narrowband and wideband channels, in both single-user and multiuser scenarios. Numerical results, including the equivalent signal-to-noise ratio per bit post-equalization, demonstrate that full-dimension one-bit digital chains significantly improve the efficiency of beamforming.**

***Index Terms*—Angle-of-arrival (AoA) estimation, analog beamforming, massive MIMO, millimeter wave (mmWave), multiuser communication.**

I. Introduction

Millimeter wave and mid-band frequencies are susceptible to free-space path loss and penetration losses, but they offer substantial bandwidth, and their shorter wavelengths allow for the integration of compact, high-density antenna arrays, enhancing antenna gain and improving the signal-to-noise ratio (SNR). Multiple-input multiple-output (MIMO) technology increases the effective aperture and directs transmission or reception more precisely.

Effective beamforming is crucial for ensuring efficiency and reliability in those frequencies. However, deploying high-resolution digital chains for numerous antenna elements leads to high hardware costs and energy consumption, mainly due to high-rate digital-to-analog converters/analog-to-digital converters (DACs/ADCs) [1]. A common compromise is the hybrid beamforming architecture, which typically employs far fewer digital chains than the number of transmit or receive antennas [2]. However, because analog arrays provide only weak signals until they are properly trained, the reduced dimensionality of the digital signal often requires extended pilot transmissions and feedback processes, posing challenges, particularly in mobile communication environments.

In this paper, we consider a receive architecture that incorporates a full set of digital chains with 1-bit ADCs to assist in beamforming [3]. These chains are specifically employed during the beamformer estimation stage to capture energy from all receive antennas in order to optimize the beams. In the subsequent data communication stage, traditional receive architectures, such as analog or hybrid beamforming, are employed for the remainder of the channel coherence time. This paper demonstrates the effectiveness of full-dimension 1-bit chains in enabling beamforming across diverse scenarios, ranging from single-user MIMO with analog beamforming to multiuser MIMO with hyprid beamforming. Across a wide range of SNRs, our approach requires up to a few hundred pilot symbols, which results in a very low duty cycle for beam acquisition, thereby minimizing energy consumption.

The authors are with the Department of Electrical and Computer Engineering, Northwestern University, Evanston, IL 60208. Email: linaliu2020@u.northwestern.edu, dGuo@northwestern.edu. This work was supported in part by the NSF under grant no. 2003098.

A. Related Work

Analog and digital beamforming have been extensively studied for MIMO systems (see e.g., [4]–[7]). Hybrid beamforming combines the benefits of analog and digital methods, providing a practical solution for supporting multiple data streams or users. Each digital chain may connect to all antennas [8], [9] or a subset of antennas [10]. In subarray-based architectures, multi-beam designs have been developed to steer beams toward arbitrary directions [11].

When channel state information (CSI) is unavailable, full-resolution ADCs support channel estimation methods like those in [12]–[16], while low-resolution ADCs used to reduce power consumption require specialized estimation techniques based on quantized outputs. For generalized MIMO channel models, such as complex Gaussian distributions, various techniques have been developed [17]–[20]. At mid-band and higher frequencies, the structured nature of channels allows exploitation of angular-domain sparsity to various extents. This often leads to framing the estimation process as quantized compressed sensing problems [21]–[23], which depend on well-designed pilot sequences to minimize sensing matrix coherence and generally require adequate pilot length and SNR for convergence. The Bussgang decomposition has been proposed to approximately linearize quantization effects [24]–[26], where uniform mid-rise quantization is needed for few-bit ADCs to avoid correlation matrix calculations. Alternatively, quantization effects can be modeled through likelihood functions [27]–[29]. Sparsity-regularized likelihood maximization has been addressed via expectation-maximization [27]. In narrowband channels with uniform linear arrays (ULAs), maximum-likelihood (ML) estimation has been applied to the angles of departure/arrival (AoDs/AoAs) and corresponding path coefficients, iteratively refining each path until conver-

gence [28]. Deep learning solutions have also been developed by approximating likelihood functions using sigmoid activations [29]. In narrowband systems with 1-bit ADCs, alternative methods resolve quantization effects by recovering missing amplitude information [30] or by incorporating quantization as constraints or loss functions into optimization frameworks [31], [32].

Hierarchical codebooks, consisting of low-resolution codewords for wide-angle coverage and high-resolution codewords for enhanced directional gain, have been proposed to accelerate beamforming [33], [34]. This method reduces search complexity to logarithmic order with respect to the number of antennas. However, each beamforming vector must be tested through a separate measurement, leading to substantial overhead and constrained beam resolution.

Prior works have explored joint channel estimation and beamforming [35]–[37], primarily focusing on reconstructing the full channel matrix for beamforming. In contrast, [38] proposes AoA-based channel estimation via beam scanning to enable hybrid beamforming in multiuser narrowband systems. Meanwhile, [39] employs analog beamforming based on AoA/AoD estimation for wideband point-to-point communication, optimizing beamforming to align with the AoA/AoD that maximizes overall power gain across clusters. Other designs include the deep-unfolding neural network [40]. Notably, spatial multiplexing is primarily governed by the angular-domain characteristics of the channel, which are largely independent of time-domain factors like varying transmit symbols and path delay responses. Prior work [3] leverages this property by extracting angular parameters to enable analog beamforming in a single-user MIMO scenario. In narrowband channels with a known number of well-separated paths, [3] designs the analog beamformer to incorporate all estimated AoAs. For wideband channels, [3] optimizes beamforming to target the AoA that captures the most significant energy across all clusters.

B. Contributions

Our key contributions are summarized as follows:

- We first evaluate a likelihood-based AoA estimation and beamforming in a narrowband model in a single-user MIMO scenario. Simulation results demonstrate that the proposed beamforming effectively recovers significant received energy, even with a moderately large angular spread of an unknown number of clusters.
- We then extend AoA estimation to the uplink of a multiuser system. By utilizing the distinct pilot sequences of different users, we are able to isolate individual users' AoAs. We then design analog beamforming techniques that maximize the signal-to-interference-plus-noise ratio (SINR) for each user.
- We further assess the preceding techniques within a hybrid receive architecture capable of supporting multiple users concurrently. In narrowband scenarios, this approach significantly reduce inter-user interference, achieving a sum spectral efficiency that approaches that of an ideal scenario with perfect channel state and transmit beamforming information. In wideband scenarios, it enables effective equalization to combat inter-symbol interference, achieving an SNR per bit post-equalization that closely matches the optimal performance.

C. Organization and Notations

The remainder of this paper is organized as follows. Sec. II introduces a unified model for both single-user and multiuser uplink systems. Sec. III describes a single-user likelihood-based angular-domain channel estimation method, which is evaluated in Sec. IV. Sec. V extends the techniques to multiuser systems, where the performance is eavluated in Sec. VI. Sec. VII concludes the paper.

We adopt the following convention: Let a denote a scalar, $\mathbf{a}$ a column vector, $\mathbf{A}$ a matrix, and $\mathcal{A}$ a set. $(\cdot)^T$ and $(\cdot)^H$ represent transpose and conjugate transpose, $|\cdot|$ denotes absolute value, $\mathbf{0}_M$ is an M-dimensional all-zero column vector, and $\mathbf{I}_M$ is the $M \times M$ identity matrix. $\text{sign}(\cdot)$, $\text{Re}(\cdot)$, and $\text{Im}(\cdot)$ indicate the sign, real, and imaginary parts, respectively.

II. System Model and Problem Formulation

We consider an uplink system with N_u users, each equipped with M_{t} transmit antennas and transmitting a single data stream to a common access point (AP). The AP is equipped with M_{r} receive antennas and a set of full-dimension digital chains, where each digital chain is equipped with a pair of 1-bit ADCs to process the in-phase and quadrature components of the received signals. Each communication period within the channel coherence time is divided into two stages. In the first stage, the full-dimension 1-bit chains are utilized to estimate analog beamformers to maximize each user's SINR. In the second stage, the estimated analog beams are applied for communication of the N_u data streams. In particular, when $N_u = 1$, only one analog beamformer is needed for a single digital chain equipped, eliminating the need for digital processing. When $N_u > 1$, a fully connected hybrid architecture is adopted, comprising N_u digital chains, where each analog beamformer serves a dedicated digital chain for one user. On each digital chain, a pair of high-resolution ADCs are employed, whose quantization errors are negligible. These two stages are repeated during each period, with the first stage being executed only during initial beam acquisition or beam recovery phases. A block diagram depicting the two-stage solution is shown in Fig. 1.

A. The MIMO Channel

A general wideband MIMO channel in higher frequencies can be modeled using a number of paths at different AoAs and AoDs, which typically form separated angular clusters. We assume that both the users' transmitters and the AP's receiver are equipped with uniform planar arrays (UPAs). Let M_H and M_V represent the horizontal and vertical dimensions of the UPA, respectively, such that the total number of antenna elements are given by $M = M_V \times M_H$. Then, the l-th path can be characterized by the parameters α_l, δ_l, φ_l, θ_l, ω_l, and ψ_l, representing the complex gain, delay, azimuth AoA, elevation AoA, azimuth AoD, and elevation AoD, respectively.

This article has been accepted for publication in IEEE Journal of Selected Topics in Signal Processing. This is the author's version which has not been fully edited and content may change prior to final publication. Citation information: DOI 10.1109/JSTSP.2025.3590607

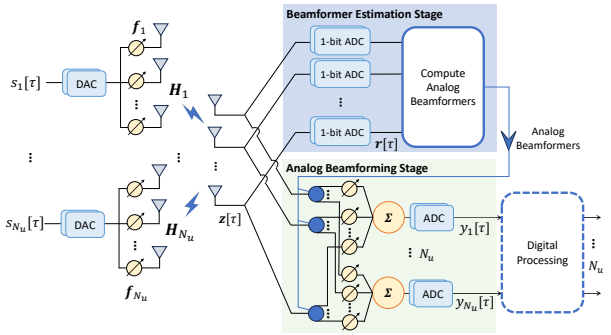

Fig. 1. The two-stage receiver: the analog beams computed in the estimation stage are applied during the communication stage.

We assume the UPA has a uniform antenna spacing of half a wavelength in both the horizontal and vertical dimensions. The UPA coordinates are defined such that φ_l, θ_l, ω_l, and ψ_l lie within the range $(-\pi/2, \pi/2)$. Define

$$\mathbf{o}_M(\theta) = [1, e^{j\pi \sin\theta}, \ldots, e^{j\pi(M-1)\sin\theta}]^T, \quad (1)$$

$$\mathbf{e}_M(\varphi, \theta) = [1, e^{j\pi \cos\theta \sin\varphi}, \cdots, e^{j\pi(M-1)\cos\theta\sin\varphi}]^T. \quad (2)$$

In general, we also use

$$\mathbf{a}_{N,M}(\varphi, \theta) = \mathbf{o}_N(\theta) \otimes \mathbf{e}_M(\varphi, \theta) \quad (3)$$

to represent the response vector of an $N \times M$ UPA to an incoming planar wave with an azimuth AoA of φ and an elevation AoA of θ, where $\otimes$ denotes the Kronecker product. For ease of notation, we introduce the following shorthand

$$\mathbf{a}_{\mathrm{r}}(\varphi, \theta) = \mathbf{a}_{M_V^{\mathrm{r}}, M_H^{\mathrm{r}}}(\varphi, \theta) \in \mathbb{C}^{M_{\mathrm{r}}} \quad (4)$$

$$\mathbf{a}_{\mathrm{t}}(\omega, \psi) = \mathbf{a}_{M_V^{\mathrm{t}}, M_H^{\mathrm{t}}}(\omega, \psi) \in \mathbb{C}^{M_{\mathrm{t}}} \quad (5)$$

to represent the response vector of the $M_V^{\mathrm{r}} \times M_H^{\mathrm{r}}$ receive UPA and the $M_V^{\mathrm{t}} \times M_H^{\mathrm{t}}$ transmit UPA, respectively. Assume that the common maximum delay spread of the channel is limited to D symbol intervals for all users. The baseband channel response for user u at lag $d \in \{0, \cdots, D-1\}$, can be represented as an $M_{\mathrm{r}} \times M_{\mathrm{t}}$ matrix:

$$\mathbf{H}_u[d] = \sum_{l_u=1}^{L_u} \alpha_{l_u} p(dT - \delta_{l_u}) \mathbf{a}_{\mathrm{r}}(\varphi_{l_u}, \theta_{l_u}) \mathbf{a}_{\mathrm{t}}^H(\omega_{l_u}, \psi_{l_u}), \quad (6)$$

where the subscript u denotes the user index, L_u is the number of propagation paths for user u, and $p(\cdot)$ accounts for the effects of pulse shaping and filtering. Let $s_u[\tau] \in \mathbb{C}$ represent the transmitted symbol in interval τ, and $\mathbf{f}_u \in \mathbb{C}^{M_{\mathrm{t}}}$ denote user u's transmit beam. In interval τ, the received signal sans noise can be expressed as

$$\mathbf{x}[\tau] = \sum_{u=1}^{N_u} \sum_{d=0}^{D-1} \mathbf{H}_u[d] \mathbf{f}_u s_u[\tau - d] \in \mathbb{C}^{M_{\mathrm{r}}}. \quad (7)$$

Let $\mathbf{w}[\tau] \sim \mathcal{CN}(\mathbf{0}_{M_{\mathrm{r}}}, \mathbf{I}_{M_{\mathrm{r}}})$ denote the additive white Gaussian noise. The unquantized received signal is given by

$$\mathbf{z}[\tau] = \mathbf{x}[\tau] + \mathbf{w}[\tau]. \quad (8)$$

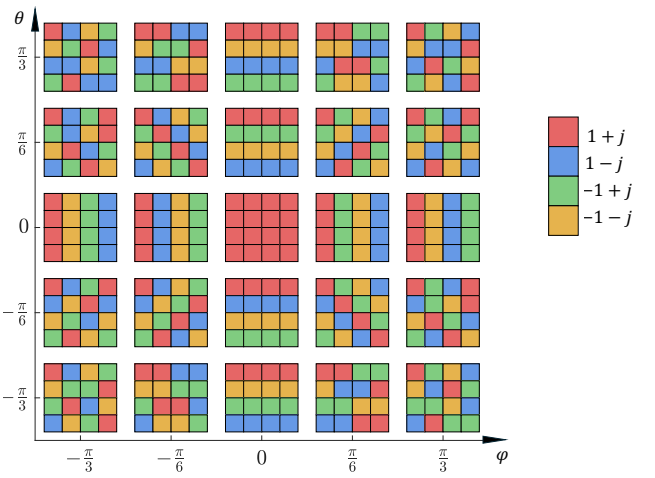

Fig. 2. Quantized noiseless output of an 4×4 UPA for AoA pairs with $\theta, \varphi \in \{-\frac{\pi}{3}, -\frac{\pi}{6}, 0, \frac{\pi}{6}, \frac{\pi}{3}\}$.

B. The Beamformer Estimation Stage

Following each receive antenna, a digital chain is equipped with a pair of 1-bit ADCs which separately quantize the in-phase and quadrature components of the received signal. The 1-bit quantization function can be described as

$$\mathcal{Q}(z) = \mathrm{sign}\left(\mathrm{Re}(z)\right) + j \cdot \mathrm{sign}\left(\mathrm{Im}(z)\right). \quad (9)$$

The element-wise quantized output in symbol interval τ (in the estimation stage) can be written as

$$\mathbf{r}[\tau] = \mathcal{Q}\left(\mathbf{z}[\tau]\right). \quad (10)$$

Although 1-bit quantization retains only the sign of the signals, spatial diversity across antenna elements allows one to infer about the channel. Fig. 2 illustrates how different AoAs result in distinct patterns in the 1-bit quantized noiseless outputs, assuming a single user, a single path, and zero delay spread. Suppose the estimation stage spans N_d symbol intervals, i.e., N_d pilot symbols are used. The goal is to extract essential channel information from the observations $\mathbf{R} = [\mathbf{r}[1], \cdots, \mathbf{r}[N_d]]$ to assist the analog beamforming.

C. The Analog Beamforming Stage

Throughout this paper, analog beamformers are implemented using phase shifters. For user u, we seek a beam $\mathbf{b}_u \in \mathbb{C}^{M_{\mathrm{r}}}$ that maximizes the SINR of the u-th digital chain's output after analog beamforming:

$$y_u[\tau] = \mathbf{b}_u^H \mathbf{z}[\tau]. \quad (11)$$

Let $\xi_{u,m}$ denote the phase of the m-th phase shifter for beam $\mathbf{b}_u$. The analog beamformer $\mathbf{b}_u \in \mathbb{C}^{M_{\mathrm{r}}}$ is determined element-wise by $b_{u,m} = e^{j\xi_{u,m}}$, $m = 1, \cdots, M_{\mathrm{r}}$. During the communication stage, $s_u[\tau]$ are assumed to be independent across τ and u, with zero mean and unit variance. The SINR of user u after analog beamforming then can be simplified as

$$\mathrm{SINR}_u = \frac{\mathbf{b}_u^H \left(\sum_{d=0}^{D-1} \mathbf{H}_u[d] \mathbf{f}_u \mathbf{f}_u^H \mathbf{H}_u^H[d] \right) \mathbf{b}_u}{\mathbf{b}_u^H \left(\sum_{v \neq u} \sum_{d=0}^{D-1} \mathbf{H}_v[d] \mathbf{f}_v \mathbf{f}_v^H \mathbf{H}_v^H[d] \right) \mathbf{b}_u + M_{\mathrm{r}}}, \quad (12)$$

since $\mathbb{E}_\tau\left[|\mathbf{b}_u^H\mathbf{w}[\tau]|^2\right] = M_{\mathrm{r}}$. For user u, we aim to solve the beamforming problem:

$$\max_{\mathbf{b}_u:\,|b_{u,1}|=\cdots=|b_{u,M_{\mathrm{r}}}|=1} \mathrm{SINR}_u. \tag{13}$$

III. Single-User Channel Estimation

In this section, we present a likelihood-based angular-domain method for single-user MIMO channel estimation. There is no need for the user index in this case. We begin with a simplified channel model with zero delay spread:

$$\mathbf{H} = \sum_{l=1}^{L} \alpha_l \mathbf{a}_{\mathrm{r}}(\varphi_l,\theta_l)\mathbf{a}_{\mathrm{t}}^H(\omega_l,\psi_l), \tag{14}$$

which is subsequently referred to as the narrowband model. The quantized output becomes

$$\mathbf{r}[\tau] = \mathcal{Q}(\mathbf{H}\mathbf{f}s[\tau] + \mathbf{w}[\tau]). \tag{15}$$

Once we develop an algorithm for this model, it shall be extended to the wideband model described by (6). Finally, we demonstrate that the developed algorithm is adaptable to non-coherent channel models, where the complex path gain α_l may vary over time in both narrowband and wideband scenarios (while other parameters $\varphi_l, \theta_l, \omega_l$ and ψ_l remain constant), with arbitrary and unknown pilot sequences.

A. Angle Estimation for Narrowband Channels

In the narrowband setting, during the estimation stage, we set $s[\tau] = 1$, for $\tau = 1, \cdots, N_d$, ensuring that $\mathbf{H}\mathbf{f}s[\tau] = \mathbf{H}\mathbf{f}$. Notably, as long as the pilot sequence consists of repetitive symbols, the algorithm remains effective, with only the SNR being affected. In the following, we first describe an algorithm under the simplifying assumption that the channel consists of a single path. We then extend the algorithm to multiple well-separated paths and demonstrate the effectiveness of the algorithm for a general channel model, where paths may be clustered.

1) A Single Path: With a single path, we omit the subscript $l = 1$ in (14). We first estimate the elevation angle θ and then use the result to estimate the azimuth angle φ. To estimate θ, we examine the received signal due to the columns of the receiver's UPA. During interval τ, let $\widetilde{\mathbf{w}}_i[\tau] \in \mathbb{C}^{M_V^{\mathrm{r}}}$ denote the additive Gaussian noise at the i-th column of the antenna array. The signal received by the i-th column is expressed as

$$\widetilde{\mathbf{r}}_i[\tau] = \mathcal{Q}\left(\zeta_i \mathbf{o}_{M_V^{\mathrm{r}}}(\theta) + \widetilde{\mathbf{w}}_i[\tau]\right), \tag{16}$$

which is a sub-vector of $\mathbf{r}[\tau]$ given by (15), where $\mathbf{o}_{M_V^{\mathrm{r}}}(\theta)$ is given by (1), and

$$\zeta_i = \alpha e^{j\pi(i-1)\cos\theta\sin\varphi}\mathbf{a}_{\mathrm{t}}^H(\omega,\psi)\mathbf{f} \tag{17}$$

represents a complex-valued coefficient. From (16), if ζ_i were known, the only remaining uncertainty in the observation, conditioned on θ, arises from the Gaussian noise. While the expression of (17) for ζ_i includes θ, the uncertainty about the other angles φ, ω, ψ allows a good approximation to assume that ζ_i follows a distribution that is not dependent on θ.

Let $\widetilde{\mathbf{R}}_i = [\widetilde{\mathbf{r}}_i[1], \cdots, \widetilde{\mathbf{r}}_i[N_d]]$ represent the received signals at the i-th column. We next focus on the likelihood $\mathcal{L}(\widetilde{\mathbf{R}}_i|\theta)$. For convenience, we define

$$f_N(\upsilon,\lambda) = \Big(Q\big(-\sqrt{2}\upsilon\big)\Big)^{\lambda}\Big(Q\big(\sqrt{2}\upsilon\big)\Big)^{N-\lambda} \tag{18}$$

where $Q(\cdot)$ denotes the Q-function. We interpret $f_N(\upsilon,\lambda)$ as the probability that, exactly λ out of N measurements of a real-valued constant υ, each corrupted by independent zero-mean Gaussian noise with variance $1/2$, are positive. For a complex-valued signal z, we define

$$\widetilde{f}_N(z,\mu,\nu) = f_N(\mathrm{Re}(z),\mu)\cdot f_N(\mathrm{Im}(z),\nu). \tag{19}$$

With model (16) in mind, we further define

$$\rho_N^m(\theta,\mu,\nu;\zeta) = \widetilde{f}_N\Big(\zeta e^{j\pi(m-1)\sin\theta},\mu,\nu\Big), \tag{20}$$

where the measurements due to the real and imaginary signal components from the m-th antenna element of a UPA column are accounted across a pilot sequence of length N. Let $\widetilde{r}_{i,m}[\tau]$ denote the m-th element of $\widetilde{\mathbf{r}}_i[\tau]$. Throughout this paper, let $H(\cdot)$ denote the Heaviside step function, i.e., $H(x) = 1$ if $x \geq 0$ and $H(x) = 0$ if $x < 0$. Then $\widetilde{\mu}_{i,m} = \sum_{\tau=1}^{N_d} H\big(\mathrm{Re}\left(\widetilde{r}_{i,m}[\tau]\right)\big)$ and $\widetilde{\nu}_{i,m} = \sum_{\tau=1}^{N_d} H\big(\mathrm{Im}\left(\widetilde{r}_{i,m}[\tau]\right)\big)$ count the numbers of positive observations in the real and imaginary parts of $\widetilde{r}_{i,m}$ across the training period, respectively. The likelihood $\mathcal{L}(\widetilde{\mathbf{R}}_i|\theta)$ can be approximated within a constant multiplier by aggregating (20) across relevant antenna elements and averaging over the distribution of ζ_i:

$$g_i(\theta) = \sum_{\zeta\in\mathcal{Z}}\prod_{m=1}^{M_V^{\mathrm{r}}} \rho_{N_d}^m\left(\theta,\widetilde{\mu}_{i,m},\widetilde{\nu}_{i,m};\zeta\right), \tag{21}$$

where we have assumed that ζ_i is uniformly distributed over $\mathcal{Z} = \left\{\beta e^{j2\pi\frac{k}{N_\zeta}}\right\}_{k=0}^{N_\zeta-1}$, where β denotes the amplitude, and N_ζ represents the number of discrete phases.[1]

Subsequently, we derive the likelihood $\mathcal{L}(\mathbf{R}|\theta)$ by combing the measurements from all UPA columns. While $\zeta_1,\ldots,\zeta_{M_H^{\mathrm{r}}}$ are correlated, we ignore their dependence to obtain the following likelihood-based objective:

$$g(\theta) = \prod_{i=1}^{M_H^{\mathrm{r}}} g_i(\theta). \tag{22}$$

Our goal is to find the optimal θ that maximizes (22). To improve the numerical accuracy of floating-point operations, we work with the logarithm of the objective value and plot it with a constant offset in later sections for convenience.

The objective function defined in (22) is nonconvex, but it typically exhibits a distinct and narrow peak around the true θ value. Leveraging this characteristic, a two-step estimation approach is proposed. Initially, we sample θ according to

$$\underline{\theta}_q = \arcsin\left(-1+(q-1)/M_V^{\mathrm{r}}\right), \quad q = 1,\ldots,2M_V^{\mathrm{r}} \tag{23}$$

[1]We estimate θ by identifying the peak locations of the likelihood-based function, which are insensitive to the assumed distribution of ζ_i. For implementation, we assume a uniform distribution with $N_\zeta = 100$ and $\beta = 0.1$, corresponding to a path SNR of -20 dB, since $|\zeta_i|^2$ controls the path SNR, as shown in (16).

and compute the corresponding objective function values. The most prominent sampling peak provides a coarse estimate, and a constrained region around it is used for fine estimation with a gradient-based algorithm. If $\check{q}$ maximizes $g\left(\underline{\theta}_q\right)$, then the constrained feasible region is set as $\left[\underline{\theta}_{\check{q}-1}, \underline{\theta}_{\check{q}+1}\right]$, and $\underline{\theta}_{\check{q}}$ serves as both a coarse estimate of θ and the initial point in the gradient-based algorithm.

Denote by $\widehat{\theta}$ the refined estimate after the preceding two-step estimation process. We substitute it into antenna response $\mathbf{a}_{\mathrm{r}}(\varphi,\theta)$ given in (3) in order to derive the likelihood for the azimuth AoA φ using a similar approach as for θ. While $\mathcal{L}(\widetilde{\mathbf{R}}|\theta)$ is derived using column-wise received signals to minimize the impact from φ, we now leverage the signals from all UPA antenna elements modeled as $\mathbf{r}[\tau] = \mathcal{Q}\left(\bar{\zeta}\mathbf{a}_{\mathrm{r}}(\varphi,\widehat{\theta}) + \mathbf{w}[\tau]\right)$, where $\bar{\zeta} = \alpha\mathbf{a}_{\mathrm{t}}^H(\omega,\psi)\mathbf{f} \in \mathbb{C}$. We then define

$$\bar{\rho}_N^m(\varphi,\theta,\mu,\nu;\zeta) = \widetilde{f}_N\left(\zeta a_m(\varphi,\theta),\mu,\nu\right), \tag{24}$$

where $a_m(\varphi,\theta)$ denotes the m-th element of the antenna response vector $\mathbf{a}_{\mathrm{r}}(\varphi,\theta)$. Let $\mu_m = \sum_{\tau=1}^{N_d} H\big(\mathrm{Re}(r_m[\tau])\big)$ and $\nu_m = \sum_{\tau=1}^{N_d} H\big(\mathrm{Im}(r_m[\tau])\big)$. The likelihood-based objective function with respect to φ can be expressed as

$$\bar{g}(\varphi) = \sum_{\zeta\in\mathcal{Z}}\prod_{m=1}^{M_{\mathrm{r}}} \bar{\rho}_{N_d}^m\left(\varphi,\widehat{\theta},\mu_m,\nu_m;\zeta\right). \tag{25}$$

We then estimate φ using the same two-step process comprising coarse sampling followed by refinement.

2) Multiple Well-Separated Paths with Known L: We introduce $\vartheta_M \approx \frac{1.78}{M-1}$, representing the angular resolution (3-dB beamwidth) for far-field radiation in a linear array with M antenna elements [41]. When the paths are separated by at least $2\vartheta_{M_V^{\mathrm{r}}}$ in the elevation angle direction and $2\vartheta_{M_H^{\mathrm{r}}}$ in the azimuth angle direction, the proposed algorithm invariably resolves individual paths with high fidelity in our experiments. Assuming the number of paths L is known a priori, we first obtain fine estimates for the L elevation angles, denoted as $\widehat{\theta}_1,\cdots,\widehat{\theta}_L$, corresponding to the L most prominent peaks of the likelihood-based function in (22). Subsequently, the azimuth angles are estimated path by path, leveraging the corresponding elevation angle estimate for each path. Specifically, φ_l for the l-th path is estimated by substituting $\widehat{\theta}_l$ into (25).

3) Clustered Paths with Unknown L: In practice, paths are not always well separated and the number of paths are unknown *a priori*. In particular, paths resulting from similar multipath propagation effects often form a cluster, sharing similar AoAs/AoDs. A single cluster may consist of up to tens of paths. The proposed algorithm remains effective in identifying the dominant path directions. Specifically, the process begins by estimating the number of separate clusters, followed by determining their dominant paths' respective AoAs. We note that closely spaced paths in the elevation (resp. azimuth) direction may contribute to a single peak in the likelihood function with respect to θ (resp. φ). In such cases, the AoA estimation may yield a compromise, reflecting the combined influence of paths with similar AoAs while still identifying a direction capable of receiving substantial energy.

In the most general case, we begin by estimating the number of paths in the elevation perspective, $\widehat{L}_\theta$, as the number of dominant peaks observed in the sampled $g(\theta)$, following sampling rule (23). A threshold-based approach is used, where peaks are counted if their values exceed a predefined threshold ϱ as a proportion of the total sum of sampled peak values. These $\widehat{L}_\theta$ peak locations provide coarse estimates of the elevation angle, which are then refined using the likelihood-based objective in (22). With the refined elevation estimates $\widehat{\theta}_l$, $l = 1,\cdots,\widehat{L}_\theta$ obtained, each $\widehat{\theta}_l$ is substituted into (25) to identify associated azimuth angles. The number of azimuth peaks for each elevation estimate is denoted as $\widehat{L}_{\varphi_l}(\geq 1)$, determined after sampling for φ based on (25). These $\widehat{L}_{\varphi_l}$ peaks are subsequently refined. Finally, the total number of identified paths is given by $\widehat{L} = \sum_{l=1}^{\widehat{L}_\theta}\widehat{L}_{\varphi_l}$, with their AoAs estimated as described.

B. Wideband and Noncoherent Channels

The proposed algorithm for narrowband angular estimation can be extended to the wideband case, where the MIMO channel matrix at different lags are described by (6). We first consider a simple scenario with a single AoA and a delay spread. By sending all 1 pilots and rearranging the parameters in (6), the signal received by the i-th column of the UPA can be expressed as (16) with

$$\zeta_i = \alpha e^{j\pi(i-1)\cos\theta\sin\varphi}\mathbf{a}_{\mathrm{t}}^H(\omega,\psi)\mathbf{f}\sum_{d=0}^{D-1} p(dT-\delta). \tag{26}$$

The channel estimation in this case then follows the same approach as in the narrowband case described in Sec. III-A.

The channel estimation described above assumes a coherent channel, where α in (6) remains constant during the channel coherence time, and repetitive pilot symbols are used. The proposed technique can be extended to accommodate arbitrary time-varying channel gains, fast fading, as well as unknown pilots, as long as the signal remains a planar wave with fixed AoAs and AoDs during the estimation period. In the remainder of this section, we develop a corresponding algorithm under the assumption of a single path. Extension and application of the algorithm to multiple well-separated paths and clustered paths follow the same approach outlined in Sec. III-A.

With $\alpha[\tau]$ and $s[\tau]$ unknown and varying over time, we can still express the signal received by the i-th column in the form of (16), but instead with a time-varying complex-valued coefficient:

$$\widetilde{\mathbf{r}}_i[\tau] = \mathcal{Q}\left(\zeta_i[\tau]\mathbf{o}_{M_V^{\mathrm{r}}}(\theta) + \widetilde{\mathbf{w}}_i[\tau]\right). \tag{27}$$

In particular, in the narrowband case, $\zeta_i[\tau] = \alpha[\tau]s[\tau]e^{j\pi(i-1)\cos\theta\sin\varphi}\mathbf{a}_{\mathrm{t}}^H(\omega,\psi)\mathbf{f}$. For the wideband case, $\zeta_i[\tau] = \alpha[\tau]e^{j\pi(i-1)\cos\theta\sin\varphi}\mathbf{a}_{\mathrm{t}}^H(\omega,\psi)\mathbf{f}\sum_{d=0}^{D-1}p(dT-\delta)s[\tau-d]$. As we need to account for the unknown $\zeta_i[\tau]$ in each time interval, we define $\widetilde{\mu}_{i,m}^{\tau} = H\big(\mathrm{Re}(\widetilde{r}_{i,m}[\tau])\big)$ and $\widetilde{\nu}_{i,m}^{\tau} = H\big(\mathrm{Im}(\widetilde{r}_{i,m}[\tau])\big)$. Using a similar approach, the likelihood-based objective for θ can be derived as

$$h(\theta) = \prod_{\tau=1}^{N_d}\prod_{i=1}^{M_H^{\mathrm{r}}}\left(\sum_{\zeta\in\mathcal{Z}}\prod_{m=1}^{M_V^{\mathrm{r}}}\rho_1^m\left(\theta,\widetilde{\mu}_{i,m}^{\tau},\widetilde{\nu}_{i,m}^{\tau};\zeta\right)\right). \tag{28}$$

This article has been accepted for publication in IEEE Journal of Selected Topics in Signal Processing. This is the author's version which has not been fully edited and content may change prior to final publication. Citation information: DOI 10.1109/JSTSP.2025.3590607

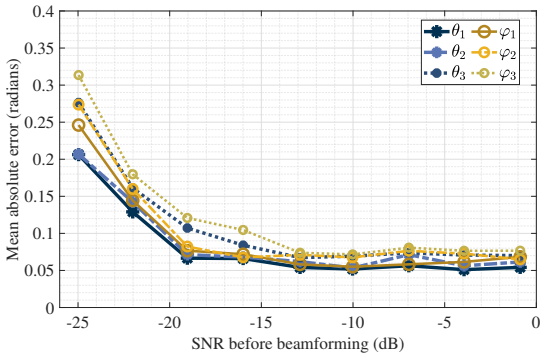

Fig. 3. Mean absolute angle estimation error vs. SNR.

After obtaining an estimate $\widehat{\theta}$, we obtain the likelihood-based objective for estimating φ as

$$\bar{h}(\varphi) = \prod_{\tau=1}^{N_d} \left(\sum_{\zeta \in \mathcal{Z}} \prod_{m=1}^{M_\mathrm{r}} \bar{\rho}_1^m \left(\varphi, \widehat{\theta}, \mu_m^\tau, \nu_m^\tau; \zeta \right) \right), \tag{29}$$

where $\mu_m^\tau = H\big(\mathrm{Re}(r_m[\tau])\big)$ and $\nu_m^\tau = H\big(\mathrm{Im}(r_m[\tau])\big)$.

IV. Single-User Analog Beamforming

In this section, we evaluate single-user analog beamforming based on estimation methods outlined in Sec. III. All numerical results are averaged over 200 random channel realizations.

A. Evaluation of Angle Estimation

We evaluate angle estimation performance in challenging wideband scenarios to demonstrate the method's effectiveness. We adopt the Urban Microcell (UMi) fast fading model from the 3GPP standard [42], focusing on non-line-of-sight propagation at a center frequency of $f_c = 28$ GHz. We consider three well-separated clusters of equal power, each consisting of 20 rays of identical power. We define the angular range as the maximum angular difference within a cluster. The angular spread is set such that the angular range is 0.19 radians in both the azimuth and elevation directions. The transmitter and receiver arrays are configured as $M_\mathrm{t} = 4\times4$ and $M_\mathrm{r} = 16\times16$, respectively. The ML-based angle estimation method is applied to identify the dominant path directions associated with the clusters. The pilot length is fixed at $N_d = 100$, and we plot the mean absolute error between the estimated cluster-wise AoAs and the true cluster centers across varying SNR regions before beamforming. As shown in Fig. 3, $N_d = 100$ suffices for SNRs ≥ -13 dB, beyond which the estimation error stabilizes. For lower SNRs, a longer pilot length can further improve accuracy. Due to the clustered nature of the channel, the estimation compromises across rays but still aligns with the cluster center, demonstrating the algorithm's ability to reliably identify cluster directions.

B. Beamforming for Narrowband Channels

In a generalized narrowband channel, we compute an analog beam that maximizes the post-beamforming SNR, which ideally solves the following optimization problem:

$$\max_{\mathbf{b}:\, |b_1| = \cdots = |b_{M_\mathrm{r}}| = 1} \left| \mathbf{b}^H \mathbf{H} \mathbf{f} \right|^2. \tag{30}$$

In the communication stage, we assume the transmitted data streams follow $s[\tau] \sim \mathcal{CN}(0,1)$, and evaluate the performance of different schemes by averaging over 1,000 symbols.

In the following, we describe three different benchmarks followed by the proposed estimation-based beamforming.

1) Ideal Beam as a Benchmark: Given perfect knowledge of CSI and transmit beam $\mathbf{f}$, the optimal solution to (30) is

$$\mathbf{b}_\mathrm{IDEAL} = \exp\left(j \angle \left(\sum_{l=1}^{L} \zeta_l \mathbf{a}_\mathrm{r}(\varphi_l, \theta_l) \right) \right). \tag{31}$$

where $\zeta_l = \alpha_l \mathbf{a}_\mathrm{t}^H(\omega_l, \psi_l)\mathbf{f}$, $\angle(\cdot)$ extracts the element-wise phases, and $\exp(\cdot)$ computes the element-wise exponentials.

2) "Strongest Beam": As another benchmark, when estimating the AoAs, we set $\widehat{L} = 1$ so that a single most prominent peak of the objective function is identified. The corresponding estimate, $\left(\widehat{\varphi}, \widehat{\theta}\right)$, is treated as the strongest beam direction, yielding a straightforward choice, which is referred to as the *strongest beam*: $\mathbf{b}_\mathrm{STR} = \mathbf{a}_\mathrm{r}\left(\widehat{\varphi}, \widehat{\theta}\right)$.

3) Hierarchical Beamformer: We also evaluate the hierarchical search method based on codebook design, an efficient approach for channel estimation and beamforming vector design, as proposed in, e.g. [43]. In this evaluation, the algorithm is adapted for UPA scenarios while keeping the transmitter side fixed, with the corresponding beamformer denoted as $\mathbf{b}_\mathrm{HIER}$.

4) Estimation-Based Beamformer: After estimating the AoAs as described in Sec. III, we compute the ML estimates of $\zeta_1, \ldots, \zeta_L$ based on the model described by (6)–(10). The resulting beam $\mathbf{b}_\mathrm{EST}$ is then obtained by plugging these estimates into (31). Instead of reconstructing the channel matrix $\mathbf{H}$, we rely on the estimates of the AoAs ($\theta_1, \ldots, \theta_L$ and $\varphi_1, \ldots, \varphi_L$) and the effective path gains ($\zeta_1, \ldots, \zeta_L$).

We evaluate the average SNRs achieved by $\mathbf{b}_\mathrm{STR}$, $\mathbf{b}_\mathrm{HIER}$, and $\mathbf{b}_\mathrm{EST}$. Specifically, we plot the "SNR ratio", which is the ratio of the SNR (in linear scale) achieved by the proposed beamformer and the SNR benchmark achieved by the ideal beam $\mathbf{b}_\mathrm{IDEAL}$. We simulate three clusters which have equal power levels, with each path within a cluster exhibiting the same SNR. The cluster AoA/AoD centers $\varphi, \theta, \omega, \psi$ are uniformly generated within $(-\pi/2 + X/2, \pi/2 - X/2)$, where $X = \varphi^\mathrm{s}$, θ^s, ω^s, and ψ^s represent the respective angular ranges. AoA centers are designed to maintain minimum separations of $1.5\vartheta_{M_V^\mathrm{r}}$ and $1.5\vartheta_{M_H^\mathrm{r}}$ at the receiver. Each cluster is assumed to consist of 10 paths. Specifically, for a cluster with L_c paths, the deviations in the elevation direction for each path relative to the cluster center are defined as $\left\{-\frac{\theta^\mathrm{s}}{2}, -\frac{\theta^\mathrm{s}}{2} + \frac{\theta^\mathrm{s}}{L_c - 1}, \ldots, \frac{\theta^\mathrm{s}}{2}\right\}$. The same applies to the the azimuth direction. Afterwards, paths are coupled randomly in terms of θ, φ pair within a cluster. Note that when $\theta^\mathrm{s} > 1.5\vartheta_{M_V^\mathrm{r}}$ or $\varphi^\mathrm{s} > 1.5\vartheta_{M_H^\mathrm{r}}$, clusters may overlap. Such overlap is not excluded in our evaluations. We set $M_\mathrm{t} = 4 \times 4$ and

This article has been accepted for publication in IEEE Journal of Selected Topics in Signal Processing. This is the author's version which has not been fully edited and content may change prior to final publication. Citation information: DOI 10.1109/JSTSP.2025.3590607

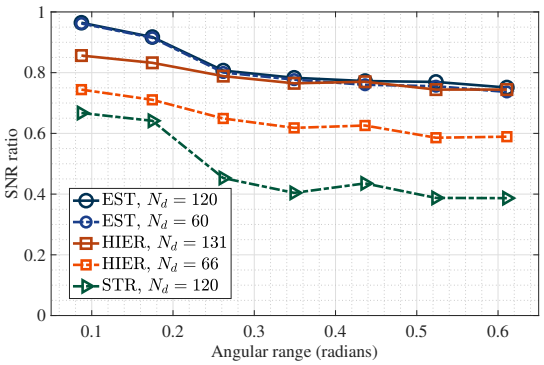

Fig. 4. SNR ratio vs. angular range for various beamforming schemes in narrowband channels.

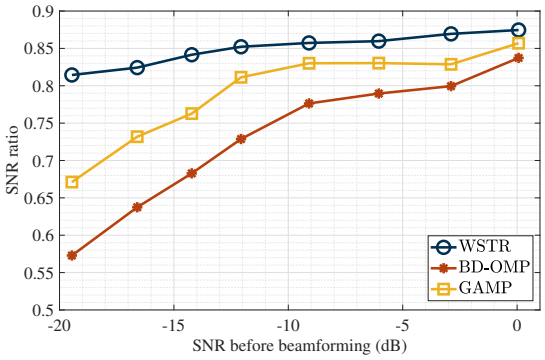

Fig. 5. SNR ratio vs. SNR before beamforming for various beamforming schemes in wideband channels.

evaluate performance for $M_{\mathrm{r}} = 16 \times 16$. For the proposed *estimation-based beamformer* (labeled as EST), we utilize $N_d = 60$ and 120 pilot symbols, respectively. The *hierarchical beamformer* (HIER) is evaluated based on the number of multipath components to estimate, with average measurement counts of 66 and 131, respectively. For the *strongest beam* (STR), $N_d = 120$ is used. The three clusters have equal power levels, with each path within a cluster exhibiting the same SNR. The average SNR per antenna before beamforming is approximately -10.7 dB, while the average SNR after *ideal beamforming* is about 13.3 dB.

Fig. 4 plots the average SNR ratios for various levels of angular range, where we set $\varphi^{\mathrm{s}} = \theta^{\mathrm{s}} = \omega^{\mathrm{s}} = \psi^{\mathrm{s}}$. The *estimation-based beamformer* outperforms both the *strongest beam* and the *hierarchical beamformer*. The *estimation-based beamformer* also demonstrates robust performance, recovering 75%–96% of the ideal SNR, even in clustered multipath environments. Despite not directly reconstructing the channel matrix or having knowledge of the transmit beam, the combination of AoA estimation and path gain estimation is sufficient to account for the joint effects of all clusters. On the other hand, the *hierarchical beamformer* demonstrates suboptimal performance; it needs significantly more measurements to achieve comparable performance.

C. Beamforming for Wideband Channels

With a wideband channel model, the SNR maximization problem can be formulated as

$$\max_{\mathbf{b}:\, |b_1|=\cdots=|b_{M_{\mathrm{r}}}|=1} \mathbf{b}^H \left(\sum_{d=0}^{D-1} \mathbf{H}[d]\mathbf{f}\mathbf{f}^H \mathbf{H}[d]^H \right) \mathbf{b}. \quad (32)$$

We set $M_{\mathrm{t}} = 4 \times 4$ and $M_{\mathrm{r}} = 8 \times 8$. We use the same UMi fast fading channel model as in Sec. IV-A, with the angular range as 0.38 radians in both azimuth and elevation directions. SNR performance is evaluated by averaging over 1,000 data symbols $s[\tau] \sim \mathcal{CN}(0, 1)$.

In the following, we describe our proposed beamforming approach and compare the resulting beamformers with those derived from estimated channels using existing methods based on quantized observations.

1) Wideband Optimal Beam as a Benchmark: Without the constant modulus constraint, the optimal solution to problem (32) is the principal eigenvector of the matrix $\sum_{d=0}^{D-1} \mathbf{H}[d]\mathbf{f}\mathbf{f}^H \mathbf{H}[d]^H$, up to a scaling factor. This digital beamformer is denoted as $\mathbf{b}_{\mathrm{WDGT}}$. With the constant modulus constraint and full channel knowledge, we propose a numerical solution as a benchmark. We initialize the beamformer phases with $\angle(\mathbf{b}_{\mathrm{WDGT}})$ and iteratively optimize each phase ξ_m for $m = 1, \ldots, M_{\mathrm{r}}$ using a block coordinate descent (BCD) algorithm, where ξ_m denotes the m-th phase component. The resulting solution is denoted as $\mathbf{b}_{\mathrm{WOPT}}$.

2) Wideband "Strongest Beam": While the matrix $\sum_{d=0}^{D-1} \mathbf{H}[d]\mathbf{f}\mathbf{f}^H \mathbf{H}[d]^H$ can be estimated by expressing $\mathbf{H}[d]\mathbf{f}$ as $\sum_{l=1}^{L} \varsigma_l p(dT - \delta_l)\mathbf{a}_{\mathbf{r}}(\varphi_l, \theta_l)$ with $\varsigma_l = \alpha_l \mathbf{a}^H(\omega_l, \psi_l)\mathbf{f}$, doing so requires estimating all path delays. As an alternative, we apply the proposed ML-based method to estimate the most prominent peak, which is treated as the dominant beam direction. The resulting beamformer is denoted as $\mathbf{b}_{\mathrm{WSTR}}$.

Prior work has investigated channel estimation from quantized observations, specifically estimating $\mathbf{H}[d]$ for $d = 0, \ldots, D-1$. Given the estimated channel and known transmit beamforming, receive beamformers can be computed accordingly. In the following, we describe two representative channel estimation methods for comparison.

3) Bussgang Decomposition-Baesd Method: With Bussgang decomposition, the quantization effect is approximated as a linear operation, enabling channel estimation by exploiting angular-domain sparsity. Techniques such as orthogonal matching pursuit (OMP) can be employed for this purpose [25]. The resulting analog beamformer is denoted as $\mathbf{b}_{\text{BD-OMP}}$.

4) Approximate Message Passing (AMP)-Based Method: The generalized AMP algorithm can be applied [22] to estimate the channel by solving the quantized compressed sensing problem. The corresponding analog beamformer, denoted as $\mathbf{b}_{\mathrm{GAMP}}$, can then be computed.

We evaluate the average SNRs achieved by $\mathbf{b}_{\mathrm{WSTR}}$, $\mathbf{b}_{\text{BD-OMP}}$, and $\mathbf{b}_{\mathrm{GAMP}}$, and plot the SNR ratio compared to the SNR benchmark achieved by $\mathbf{b}_{\mathrm{WOPT}}$. For OMP and AMP based-method, training pilot during the estimation stage is chosen as Zadoff-Chu sequence. We test over different SNR regions before beamforming. In Fig. 5, as SNR increases, N_d is set to $80, 60, 40, 40, 30, 20, 10$, and 8, respectively. Unlike existing methods that estimate the full channel and require knowledge

This article has been accepted for publication in IEEE Journal of Selected Topics in Signal Processing. This is the author's version which has not been fully edited and content may change prior to final publication. Citation information: DOI 10.1109/JSTSP.2025.3590607

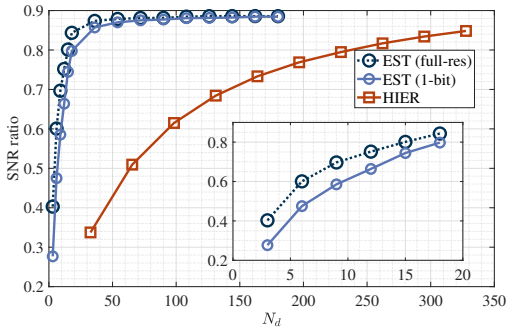

(a) Narrowband setting.

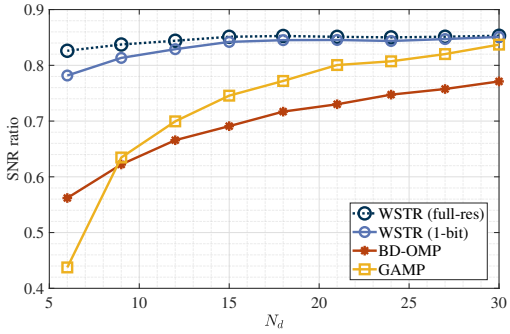

(b) Wideband setting.

Fig. 6. SNR ratio vs. N_d.

of the transmit beamforming, our approach only estimates the AoAs and does not rely on any transmit beam information. Remarkably, our method outperforms both the Bussgang-based OMP and the Generalized AMP approaches.

D. Efficiency Comparison

We evaluate the beamforming SNR performance against the number of pilot symbols for different schemes.

In the narrowband case, we compare our *estimation-based beamforming* with hierarchical beamforming, which does not rely on full-dimension digital chains. Hierarchical beamforming requires more than $L(2^{S_0} - 2S_0 + 2\log_2 M_{\rm r})$ measurements, where L is the number of paths and S_0 is the index of the initial search layer [43]. At low-to-moderate SNRs, limited gain from low-resolution codewords demands a finer beam resolution (larger S_0). Moreover, increasing $M_{\rm r}$ further raises the overhead. In the wideband case, we compare our beamformers with those obtained via existing channel estimation methods, assuming the same full-dimension 1-bit ADC receiver architecture. As an additional benchmark, we replace 1-bit ADCs with full-resolution ADCs at the receiver. This removes quantization effects in the beamformer estimation stage. We compute the analog beamformers accordingly in both narrowband and wideband cases. To distinguish between configurations, we label the results with "1-bit" and "full-res", respectively.

Fig. 6(a) shows the SNR ratio versus pilot length in the narrowband case, where the channel model follows the description in Sec. IV-B with an angular range of 0.26 radians. The pre-beamforming SNR is -12.24 dB, and the post-beamforming SNR is 11.11 dB. By exploiting spatial diversity through large M_r, our method enables significantly faster beamforming than hierarchical beamforming. The wideband channel model is based on Sec. IV-C, with an angular range of 0.19 radians. The pre-beamforming SNR is -8.53 dB, and the post-beamforming SNR is 8.87 dB. Fig. 6(b) presents the wideband case. Under the same full-dimension digital chain configuration, our method requires far fewer pilot symbols to achieve comparable SNR after beamforming, outperforming existing channel estimation-based approaches. Notably, the 1-bit ADC system performs closely to the full-resolution ADC baseline, requiring fewer than 10 additional pilot symbols.

Our approach focuses on receiver-side beamforming design and can be effectively applied when reasonable transmit beamforming is in place. Under such conditions, energy concentration in the angular domain allows for reliable AoA estimation and efficient analog beamforming.

E. Computational Complexity

We focus on the coherent channel setting, which is more relevant to beamforming. In this case, measurements only affect the calculation of certain exponent terms used in evaluating the objective functions. These include $\widetilde{\mu}_{i,m}, \widetilde{\nu}_{i,m}$ for $g(\theta)$ and μ_m, ν_m for $\bar{g}(\varphi)$ (e.g., in (21)). Computing these exponent terms involves a complexity of $O(M_{\rm r}N_d)$. Once computed, the subsequent likelihood evaluations' complexity are independent of N_d. Given these exponents, in both narrowband and wideband scenarios, evaluating $g(\theta)$ in (22) has a complexity of $O\left(M_{\rm r}N_\zeta\right)$. Coarse sampling over $M_V^{\rm r}$ elevation angles incurs $O(M_V^{\rm r}M_{\rm r}N_\zeta)$ complexity. Gradient descent is then applied to $\widehat{L}_\theta$ coarse elevation estimates, with gradients computed numerically. Suppose each gradient descent implementation requires $I_{\rm g}$ iterations for convergence. The total cost for elevation angle estimation is thus $O\left((M_V^{\rm r} + I_{\rm g}\widehat{L}_\theta)M_{\rm r}N_\zeta\right)$. Similarly, the complexity for azimuth angle estimation is $O\left((M_H^{\rm r} + I_{\rm g}\widehat{L})M_{\rm r}N_\zeta\right)$.

For *estimation-based beamforming* in the narrowband case, we estimate both amplitude and phase of the effective path gain ζ for each $(\widehat{\theta},\widehat{\varphi})$ pair, requiring $O\left(I_{\rm g}\widehat{L}M_{\rm r}\right)$ for all $\widehat{L}$ paths. The total complexity hence becomes $O\left(\left(M_V^{\rm r} + M_H^{\rm r} + I_{\rm g}\widehat{L}\right)M_{\rm r}N_\zeta + M_{\rm r}N_d\right)$. In the wideband case with "*strongest beam*" ($\widehat{L}_\theta = \widehat{L} = 1$), the complexity simplifies to $O\left(\left(M_V^{\rm r} + M_H^{\rm r} + I_{\rm g}\right)M_{\rm r}N_\zeta + M_{\rm r}N_d\right)$.

In the wideband scenarios, the complexity of the Bussgang decomposition-based method is $O\left(I_{\rm b}^4 + I_{\rm b}(N_d^2M_{\rm r}^2 + DN_dM_{\rm r}^2M_{\rm t})\right)$, where $I_{\rm b}$ is the number of OMP iterations [25]. For the AMP-based method, the complexity is $O\left(I_{\rm a}DN_dM_{\rm r}^2M_{\rm t}\right)$, where $I_{\rm a}$ denotes the AMP iteration count [44]. In contrast, our method is independent of the number of transmit antennas ($M_{\rm t}$) and scales linearly with $(M_V^{\rm r} + M_H^{\rm r})M_{\rm r}$ instead of $M_{\rm r}^2$, offering better scalability.

F. Comparison to Digital Beamforming

To provide a more comprehensive evaluation, we compare the analog beamformer with the digital beamformer. For fair

This article has been accepted for publication in IEEE Journal of Selected Topics in Signal Processing. This is the author's version which has not been fully edited and content may change prior to final publication. Citation information: DOI 10.1109/JSTSP.2025.3590607

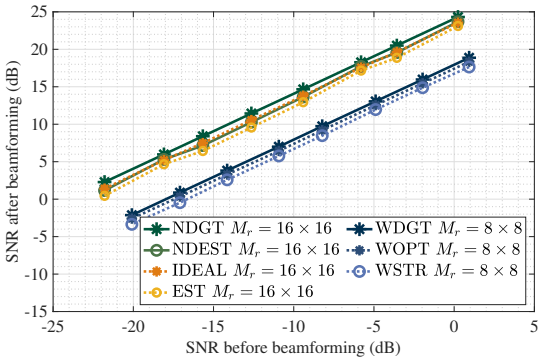

Fig. 7. SNR after beamforming vs. SNR before beamforming.

comparison, we consider the constraint for digital beamforming as $\mathbf{b} : \|\mathbf{b}\|^2 = M_{\mathrm{r}}$.

1) Narrowband Digital Beamformer: Assuming perfect CSI and transmit beamformer $\mathbf{f}$, the optimal digital receive beamformer, denoted by $\mathbf{b}_{\mathrm{NDGT}}$, is a scaled version of $\mathbf{Hf}$. Since $\mathbf{Hf} = \sum_{l=1}^{L} \zeta_l \mathbf{a}_{\mathrm{r}}(\varphi_l, \theta_l)$, we estimate it via our ML-based method when $\mathbf{H}$ and $\mathbf{f}$ are unknown, yielding the estimated digital beamformer $\mathbf{b}_{\mathrm{NDEST}}$.

2) Wideband Digital Beamformer: We have introduced the ideal digital beamformer $\mathbf{b}_{\mathrm{WDGT}}$ when discussing *wideband optimal beam* in Sec. IV-C. To estimate the corresponding digital beamformer via channel estimation, we will need to compute $\mathbf{H}[d]\mathbf{f}$ for different delay taps. As shown in Fig. 5, the *wideband "strongest beam"* performs close to the *wideband optimal beam* while requiring significantly less computation, i.e., only the AoA of the dominant path is needed. Thus, we bypass multi-path AoA and delay estimation and directly compare performance against $\mathbf{b}_{\mathrm{WSTR}}$. This delay estimation problem will later be addressed in the wideband multiuser setting in Sec. V-B.

The narrowband channel model is based on the description in Sec.IV-B, with an angular range of 0.26 radians. The wideband channel model follows Sec.IV-C, with an angular range of 0.19 radians. We plot the average SNR after beamforming achieved by $\mathbf{b}_{\mathrm{NDGT}}, \mathbf{b}_{\mathrm{NDEST}}, \mathbf{b}_{\mathrm{IDEAL}}, \mathbf{b}_{\mathrm{EST}}, \mathbf{b}_{\mathrm{WDGT}}, \mathbf{b}_{\mathrm{WOPT}}$ and $\mathbf{b}_{\mathrm{WSTR}}$ in Fig. 7. While digital beamforming offers greater flexibility, the improvement in beamforming gain is modest, i.e., approximately 0.83 dB in the narrowband case and 0.52 dB in the wideband case. In the narrowband case, we have shown that our method extends naturally to digital beamforming. In the wideband case, the estimated $\mathbf{b}_{\mathrm{WSTR}}$ achieves competitive performance to $\mathbf{b}_{\mathrm{WDGT}}$ with a modest gap of approximately 1.22 dB. The gap between the narrowband and wideband curves primarily stems from the different beamforming gains resulting from the different receive UPA sizes.

V. Multiuser Channel Estimation

Assume each user u transmits a random pilot $s_u[\tau]$ as an independent random binary phase-shift keying (BPSK) symbol for $\tau = 1, \cdots, N_d$. We show that the angular-domain channel estimation method introduced in Sec. III can be extended to the multiuser scenario and achieve good performance.

A. Angle Estimation for Narrowband Channels

We first consider a simplified scenario with two users, each with a single path. The relevant parameters are therefore directly indexed by user u. For user $u \in \{1, 2\}$, define

$$\varsigma_{u,i} = \alpha_u e^{j\pi(i-1)\cos\theta \sin\varphi} \mathbf{a}_{\mathrm{t}}^H(\omega_u, \psi_u)\mathbf{f}_u. \tag{33}$$

Following (16), we write

$$\begin{aligned}\widetilde{r}_{i,m}[\tau] = \mathcal{Q}\Big(&\varsigma_{1,i} s_1[\tau] e^{j\pi(m-1)\sin\theta_1} \\ &+ \varsigma_{2,i} s_2[\tau] e^{j\pi(m-1)\sin\theta_2} + \widetilde{w}_{i,m}[\tau]\Big),\end{aligned} \tag{34}$$

where $\widetilde{w}_{i,m}$ is the m-th element of $\widetilde{\mathbf{w}}_i$. We assume that $\varsigma_{1,i}$ and $\varsigma_{2,i}$ are uniformly distributed over discrete sets of sizes $N_{\varsigma_{1,i}}$ and $N_{\varsigma_{2,i}}$, respectively, while $\theta_2 \sim \mathrm{Uniform}(-\pi/2, \pi/2)$. Computing the likelihood $\mathcal{L}\left(\widetilde{\mathbf{R}}_i | \theta_1, \mathbf{s}_1\right)$ as by averaging the interfering user's parameters is rather complicated. Since the contribution of user 2's information diminishes in the conditional likelihood function, when conditioned on θ_1 and $s_1[\tau]$, we take the approximation

$$\widetilde{r}_{i,m}[\tau] \cong \mathcal{Q}\left(\varsigma_{1,i} s_1[\tau] e^{j\pi(m-1)\sin\theta_1} + \breve{w}_{i,m}[\tau]\right), \tag{35}$$

where user 2's signal is treated as white noise and absorbed into the noise component $\breve{w}_{i,m}[\tau]$. Using the symmetry $\mathcal{Q}(-z) = -\mathcal{Q}(z)$ for all $z \in \mathbb{C}$ and the fact that the BPSK pilot symbols $s_u[\tau] \in \{-1, 1\}$ are known, we introduce $\check{r}_{u,i,m}[\tau] = s_u[\tau]\widetilde{r}_{i,m}[\tau]$ to write a statistically equivalent model for user u:

$$\check{r}_{u,i,m}[\tau] \cong \mathcal{Q}\left(\varsigma_{u,i} e^{j\pi(m-1)\sin\theta_u} + \breve{w}_{i,m}[\tau]\right). \tag{36}$$

This approximation is also applicable to scenarios with $N_u > 2$ users, each with multiple paths. The complete received signal at time τ is expressed as $\mathbf{r}[\tau] = \mathcal{Q}\left(\sum_{u=1}^{N_u} \mathbf{H}_u \mathbf{f}_u s_u[\tau] + \mathbf{w}[\tau]\right)$ with the measurements from the i-th column of the UPA denoted as $\widetilde{\mathbf{r}}_i[\tau]$. As in the single-user case in Sec. III, even when the user has multiple paths, the likelihood-based objective conditioned on a single path is utilized to detect the directions of all dominant paths. Let $\check{\mathbf{R}}_{u,i} = [\check{\mathbf{r}}_{u,i}[1], \cdots, \check{\mathbf{r}}_{u,i}[N_d]]$, where $\check{\mathbf{r}}_{u,i}[\tau] = s_u[\tau]\widetilde{\mathbf{r}}_i[\tau]$. Following Sec. III-A, the likelihood for the elevation angle θ of user u with known pilot sequence $\mathbf{s}_u$ is approximated as:

$$\mathcal{L}(\check{\mathbf{R}}_{u,i} | \theta) \propto g_{u,i}(\theta) \tag{37}$$

$$= \sum_{\varsigma \in \mathcal{Z}} \prod_{m=1}^{M_V^{\mathrm{r}}} \rho_{N_d}^m\left(\theta, \check{\mu}_{u,i,m}, \check{\nu}_{u,i,m}; \varsigma\right), \tag{38}$$

where $\check{\mu}_{u,i,m} = \sum_{\tau=1}^{N_d} H\big(\mathrm{Re}(\check{r}_{u,i,m}[\tau])\big)$ and $\check{\nu}_{u,i,m} = \sum_{\tau=1}^{N_d} H\big(\mathrm{Im}(\check{r}_{u,i,m}[\tau])\big)$. Combining the likelihoods due to all columns of the UPA, we arrive at the following likelihood-based objective function for the elevation angle of user u:

$$g_u(\theta) = \prod_{i=1}^{M_H^{\mathrm{r}}} g_{u,i}(\theta). \tag{39}$$

The effectiveness of this approximation is demonstrated in Fig. 8, where there are two users, each with two well-separated paths in the elevation direction. The results demonstrate that

This article has been accepted for publication in IEEE Journal of Selected Topics in Signal Processing. This is the author's version which has not been fully edited and content may change prior to final publication. Citation information: DOI 10.1109/JSTSP.2025.3590607

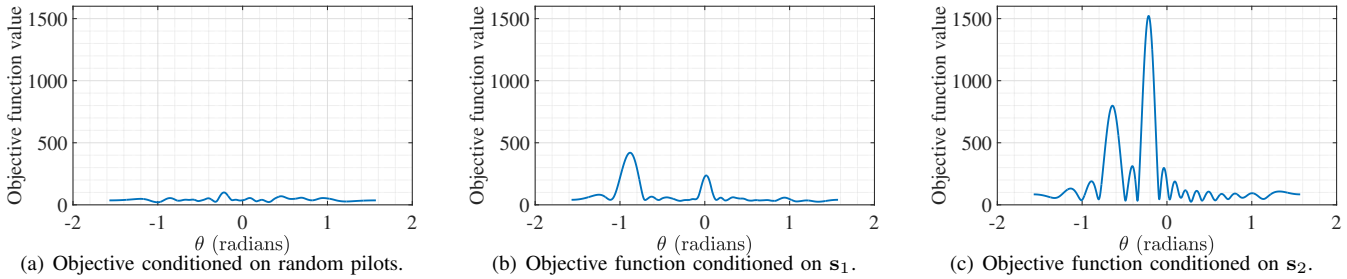

(a) Objective conditioned on random pilots. (b) Objective function conditioned on $\mathbf{s}_1$. (c) Objective function conditioned on $\mathbf{s}_2$.

Fig. 8. Simulation settings: $M_{\rm t} = 4 \times 4$ for each user, $M_{\rm r} = 16 \times 16$, and $N_d = 100$. Path SNRs: -15 dB, -20 dB for user 1 and -5 dB, -10 dB for user 2. True θ's: -0.8745, 0.0154 for user 1 and -0.2162, -0.6413 for user 2. (a) Conditioned on a random pilot sequence independent of both $\mathbf{s}_1$ and $\mathbf{s}_2$, the objective function remains small. (b) Conditioning on user 1's pilots yields prominent peaks at -0.8809 and 0.0165. (c) Conditioning on user 2's pilots yields prominent peaks at -0.2161 and -0.6420.

even with very different signal strengths between the users, the approximation in (36) remains valid and aids in the angular domain estimation.

With the estimate $\widehat{\theta}$, the same approximation applies to φ. Let $\bar{\mathbf{r}}_u[\tau] = s_u[\tau]\mathbf{r}[\tau]$, with $\bar{r}_{u,m}[\tau]$ being the m-th element of $\bar{\mathbf{r}}_u[\tau]$. The associated objective function follows (25) as

$$\bar{g}_u(\varphi) = \sum_{\varsigma \in \mathcal{Z}} \prod_{m=1}^{M_{\rm r}} \bar{\rho}_{N_d}^m \left(\varphi, \widehat{\theta}, \bar{\mu}_{u,m}, \bar{\nu}_{u,m}; \varsigma\right) \tag{40}$$

where $\bar{\mu}_{u,m} = \sum_{\tau=1}^{N_d} H\big(\mathrm{Re}(\bar{r}_{u,m}[\tau])\big)$ and $\bar{\nu}_{u,m} = \sum_{\tau=1}^{N_d} H\big(\mathrm{Im}(\bar{r}_{u,m}[\tau])\big)$.

In the preceding narrowband scenario, multiple paths are handled using the same procedure outlined in Sec. III-A.

B. Angle Estimation for Wideband Channels

For wideband channels, the analysis for each user u begins with a single-path scenario. Extending this to multiple paths requires additional considerations, particularly when accounting for pilot sequences during the likelihood derivation, as asynchrony arises from unknown delay taps. We focus on the case of well-separated paths for illustration, which can be seamlessly applied to identify dominant paths from separated clusters. Given that the exact number of clusters or paths for user u is unknown, the objective is to identify the $\widehat{L}_u$ most well-separated dominant paths.

1) A Single Path per User: We aim to express the signal received by the i-th column in the form of (16). With some rearrangement, conditioned on θ_u and $s_u[\tau]$, we take the approximation

$$\widetilde{\mathbf{r}}_i[\tau] \cong \mathcal{Q}\left(\varsigma_{u,i}\widetilde{s}_u[\tau]\mathbf{o}_{M_V^{\rm t}}(\theta_u) + \check{\mathbf{w}}_i[\tau]\right), \tag{41}$$

where $\varsigma_{u,i}$ is given in (33),

$$\widetilde{s}_u[\tau] = \sum_{d=0}^{D-1} p(dT - \delta_u) s_u[\tau - d], \tag{42}$$

and all other users' signals are treated as white noise and absorbed into the noise component $\check{\mathbf{w}}_i[\tau]$. Since user identity and its association with the corresponding AoA estimates rely on the users' pilot sequences, we aim to use the true $\widetilde{s}_u[\tau]$ values, which incorporates pilot information, while assuming a uniform distribution only for $\varsigma_{u,i}$ when deriving the likelihood-based objective. While $\mathbf{s}_u$ is known, the knowledge of $\widetilde{\mathbf{s}}_u$ depends on the pulse shaping effect, as well as the unknown parameters D and δ_u. We assume that the pulse shaping function is known at the AP. We then use an estimated value $\widehat{D}$, chosen to be large enough such that it exceeds the true D value with high probability.[2] Afterwards, we estimate δ_u to enable further analysis. To minimize computational complexity, discrete values of δ_u are evaluated, and the optimal estimate, denoted as $\widehat{\delta}_u$, is selected. This optimal value $\widehat{\delta}_u$, together with $\widehat{D}$, is then substituted into (42) to compute the approximate $\widetilde{s}_u[\tau]$, which is subsequently used to derive the conditional likelihood functions.

The discrete test set for δ_u is defined as $\mathcal{D} = \left\{0, T/\varepsilon, \cdots, (\varepsilon-1)T/\varepsilon, T, \cdots, (\widehat{D}-1)T\right\}$, where $\varepsilon > 1$ can be tuned. When $\widehat{D}$ and ε are sufficiently large, the set $\mathcal{D}$ will contain a value that closely approximate the true δ_u. With this close estimate, the corresponding likelihood-based objective typically yields a prominent peak near the true AoA in both the elevation and azimuth angles. Note that while choosing a large $\widehat{D}$ increases computational complexity, it does not compromise estimation accuracy. A larger $\widehat{D}$ ensures that the true δ_u is included in the tested range without prematurely truncating the search region. On the other hand, using a larger $\widehat{D}$ will not significantly affect the accuracy of $\widetilde{s}_u[\tau]$ calculation. This is because the light-tailed nature of a typical pulse shaping function $p(dT - \delta_u)$, such as the raised cosine-filter [45], [46]. Consequently, the term $p(dT - \delta_u)s[\tau - d]$ has minimal impact on $\widetilde{s}_u[\tau]$ when d is large for a given δ_u.

We now describe the selection of $\widehat{\delta}_u$ in detail. Given the true δ_u, the likelihood-based objective exhibits a prominent peak. Therefore, the goal is to select a $\widehat{\delta}_u$ that maximizes the prominence of the peak in the derived likelihood function among all candidate values. With argument δ, we first derive the corresponding likelihood-based objective conditioned on θ and the calculated $\widetilde{\mathbf{s}}_u(\delta) = [\widetilde{s}_u(\delta)[1], \cdots, \widetilde{s}_u(\delta)[N_d]]$, as a function of θ and δ. We observe that (41) represents a

[2]We can estimate the value of D based on the propagation environment and system settings. For instance, according to the clustered delay line (CDL)-C channel model, $\delta = \delta_{\rm normalized} \times \mathrm{DS}_{\rm desired}$, with $\delta_{\rm normalized}$ ranging from 0 to 8.6523. For a nominal delay spread with $\mathrm{DS}_{\rm desired} = 100$ ns and a 10 MHz bandwidth, D is calculated as 9. Therefore, setting $\widehat{D} = 15$ provides a sufficient estimate, even for environments with rich multipath propagation.

This article has been accepted for publication in IEEE Journal of Selected Topics in Signal Processing. This is the author's version which has not been fully edited and content may change prior to final publication. Citation information: DOI 10.1109/JSTSP.2025.3590607

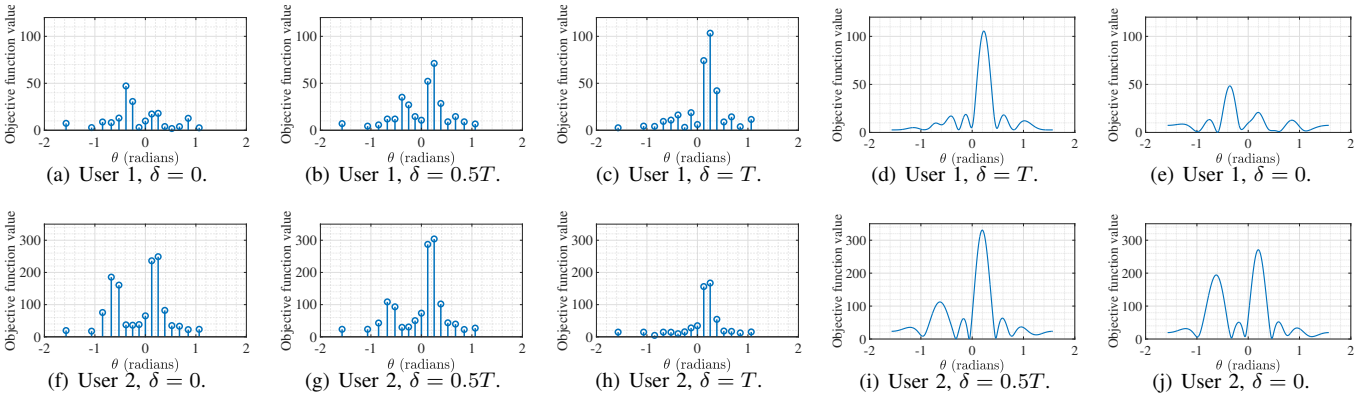

(a) User 1, $\delta = 0$. (b) User 1, $\delta = 0.5T$. (c) User 1, $\delta = T$. (d) User 1, $\delta = T$. (e) User 1, $\delta = 0$.

(f) User 2, $\delta = 0$. (g) User 2, $\delta = 0.5T$. (h) User 2, $\delta = T$. (i) User 2, $\delta = 0.5T$. (j) User 2, $\delta = 0$.

Fig. 9. Simulation settings: $M_{\rm t} = 4 \times 4$ for both users, $M_{\rm r} = 8 \times 8$, $N_d = 200$. Path parameters: User 1 has path 1 with -15 dB, path 2 with -20 dB; $\theta_1 = 0.2270$, $\theta_2 = -0.3335$; $\delta_1 = 0.9879T$, $\delta_2 = 0.0998T$. User 2 has path 1 with -5 dB, path 2 with -10 dB; $\theta_1 = 0.1954$, $\theta_2 = -0.6202$; $\delta_1 = 0.4532T$, $\delta_2 = 0.0662T$. (a)-(c): For User 1, the two largest peaks for sampled (θ, δ) pairs with distinct θ's are $(\bar{\theta}_1 = 0.2527, \widehat{\delta}_1 = T)$ and $(\bar{\theta}_2 = -0.3844, \widehat{\delta}_2 = 0)$. (d) and (e): Likelihood functions conditioned on $\widetilde{\mathbf{s}}_1$ with $\widehat{\delta}_1 = T$ and $\widehat{\delta}_2 = 0$ yield refined estimates of $\widehat{\theta}_1 = 0.2262$ and $\widehat{\theta}_2 = -0.3581$, respectively, through refinement around $\bar{\theta}_1$ and $\bar{\theta}_2$. (f)-(h): For user 2, the two largest peaks for sampled (θ, δ) pairs with distinct θ's are $(\bar{\theta}_1 = 0.2527, \widehat{\delta}_1 = 0.5T)$ and $(\bar{\theta}_2 = -0.6751, \widehat{\delta}_2 = 0)$. (i) and (j): Likelihood functions conditioned on $\widetilde{\mathbf{s}}_2$ with $\widehat{\delta}_1 = 0.5T$ and $\widehat{\delta}_2 = 0$ yield refined estimates of $\widehat{\theta}_1 = 0.1964$ and $\widehat{\theta}_2 = -0.6236$, respectively, through refinement around $\bar{\theta}_1$ and $\bar{\theta}_2$.

combination of models (16) and (27) in the sense that the coefficient of $\mathbf{o}_{M_V^{\rm r}}(\theta_u)$ consists of a time-invariant component $\varsigma_{u,i}$ and a time-varying component $\widetilde{s}_u[\tau]$. Consequently, the likelihood-based function can be derived by accounting for $\widetilde{s}_u(\delta)[\tau]$ in each time interval, while assuming a uniform distribution for $\varsigma_{u,i}$ after considering all N_d measurements across the i-th column of the UPA, yielding

$$h_u(\theta, \delta) = \prod_{i=1}^{M_H^{\rm r}} \left(\sum_{\varsigma \in \mathcal{Z}} \prod_{\tau=1}^{N_d} \prod_{m=1}^{M_V^{\rm r}} \rho_1^m \left(\theta, \widetilde{\mu}_{i,m}^{\tau}, \widetilde{\nu}_{i,m}^{\tau}; \varsigma \widetilde{s}_u(\delta)[\tau] \right) \right). \tag{43}$$

Using (43), we first quantize both θ and δ to find the optimal pair. We evaluate all combinations of $\delta \in \mathcal{D}$ and $\underline{\theta}_q$ for $q = 1, \cdots, 2M_V^{\rm r}$, resulting in $2M_V^{\rm r}\big(\varepsilon(\widehat{D} - 1) + 1\big)$ pairs. Each combination is substituted into (43) to compute the corresponding objective value. The pair $(\bar{\theta}_u, \widehat{\delta}_u)$ is selected as the maximizer of $h_u(\theta, \delta)$ among all tested combinations, where $\widehat{\delta}_u$ is the discrete delay estimate for user u. Using $\widehat{\delta}_u$, we derive the likelihood function for θ, denoted as $h_u(\theta, \widehat{\delta}_u)$. Afterwards, $\bar{\theta}_u$ provides a coarse estimate and serves as the initial point for gradient-based refinement utilizing $h_u(\theta, \widehat{\delta}_u)$, yielding the refined estimate $\widehat{\theta}_u$.

Once we obtain $\widehat{\theta}_u$, we can estimate φ using the following objective function:

$$\bar{h}_u(\varphi) = \sum_{\varsigma \in \mathcal{Z}} \prod_{\tau=1}^{N_d} \prod_{m=1}^{M_{\rm r}} \bar{\rho}_1^m \left(\varphi, \widehat{\theta}_u, \mu_m^{\tau}, \nu_m^{\tau}; \varsigma \widetilde{s}_u(\widehat{\delta}_u)[\tau] \right), \tag{44}$$

which is derived as a combination of (25) and (29).

2) Multiple Well-separated Paths per User: When user u has well-separated paths, the goal is to identify the $\widehat{L}_u$ distinct AoA pairs corresponding to prominent peaks in the likelihood-based objective function.

We first use (43) to estimate $\widehat{L}_u$ elevation angles. Specifically, we evaluate all combinations of $\delta \in \mathcal{D}$ and $\underline{\theta}_q$ for $q = 1, \cdots, 2M_V^{\rm r}$, yielding $2M_V^{\rm r}\big(\varepsilon(\widehat{D} - 1) + 1\big)$ objective values. From these, we select the $\widehat{L}_u$ pairs of (θ, δ) that have the largest objective values with distinct θ values, denoted as $(\bar{\theta}_{l_u}, \widehat{\delta}_{l_u}), l_u = 1, \cdots, \widehat{L}_u$. While each path typically has a unique delay, the discrete candidate set $\mathcal{D}$ may lead to duplicate delay estimates for $\widehat{\delta}_{l_u}$. For each l_u, we substitute $\widehat{\delta}_{l_u}$ into (43) to obtain the likelihood function $h_u(\theta, \widehat{\delta}_{l_u})$. The coarse estimate $\bar{\theta}_{l_u}$ is then refined using $h_u(\theta, \widehat{\delta}_{l_u})$ with a gradient-based method, yielding the elevation angle estimate $\widehat{\theta}_{l_u}$. Finally, φ_{l_u} is estimated using (44) by substituting the corresponding $\bar{\theta}_{l_u}$.

The estimation process for θ and δ is illustrated in Fig. 9, considering two users, each with two paths, and $D = 2$. For simplicity in illustration, we set $\widehat{D} = \widehat{L}_1 = \widehat{L}_2 = \varepsilon = 2$. We have verified via such experiments that the proposed approach enables the estimation of AoA pairs for the $\widehat{L}_u$ paths with high fidelity.

The multiuser wideband angular-domain estimation method naturally extends to scenarios with clustered paths. In such cases, dominant paths within separate clusters are identified, accounting for the combined effect of closely spaced AoAs. A potential concern occurs when clusters have similar AoA pairs but different delays, possibly causing paths from distinct clusters to be treated as a single path. However, as long as the correct AoA is detected, beamforming will still capture energy from that direction.

VI. Multiuser Analog Beamforming

This section evaluates the performance of analog beamforming based on the angle estimates in Sec. V and examines its impact on overall signal processing at the receiver.

A. Beamforming for Narrowband Channels

In the narrowband case, given an analog beam for user u, $\mathbf{b}_u$, the SINR maximization problem follows (12) and (13):

$$\max_{\mathbf{b}_u : |b_{u,1}| = \cdots = |b_{u,M_{\rm r}}| = 1} \frac{\left| \mathbf{b}_u^H \mathbf{H}_u \mathbf{f}_u \right|^2}{\sum\limits_{v \neq u} \left| \mathbf{b}_u^H \mathbf{H}_v \mathbf{f}_v \right|^2 + \mathbf{b}_u^H \mathbf{b}_u}. \tag{45}$$

This article has been accepted for publication in IEEE Journal of Selected Topics in Signal Processing. This is the author's version which has not been fully edited and content may change prior to final publication. Citation information: DOI 10.1109/JSTSP.2025.3590607

1) Optimal Beamformer: Without the constant modulus constraint on phase shifters, this problem admits a closed form solution $\mathbf{b}_u^0 = \left(\mathbf{I}_{M_\mathrm{r}} + \sum_{v\neq u} \mathbf{H}_v \mathbf{f}_v \mathbf{f}_v^H \mathbf{H}_v^H\right)^\dagger \mathbf{H}_u \mathbf{f}_u$ up to a scalar factor [47]. Under the constant modulus constraint and assuming full channel knowledge, we optimize the beamformer phases using the BCD algorithm, initialized with $\angle(\mathbf{b}_u^0)$. The obtained solution is denoted as $\mathbf{B}^{\text{opt}} = [\mathbf{b}_1^{\text{opt}}, \cdots, \mathbf{b}_{N_u}^{\text{opt}}]$.

2) Estimation-Based Beamformer: Without channel knowledge, we estimate the AoAs of dominant paths. Introducing $\varsigma_{l_u} = \alpha_{l_u} \mathbf{a}_\mathrm{t}^H(\omega_{l_u}, \psi_{l_u}) \mathbf{f}_u$,

$$\mathbf{H}_u \mathbf{f}_u = \sum\nolimits_{l_u} \varsigma_{l_u} \mathbf{a}_\mathrm{r}(\varphi_{l_u}, \theta_{l_u}). \tag{46}$$

Given the estimated number of dominant paths and φ, θ estimates following Sec. V-A, we determine the corresponding ML estimate of ς_{l_u}. These parameters suffice for analog beamforming computation, eliminating the need to reconstruct the full channel matrix. Following the methodology of optimal beamforming, we plug in the estimates instead. Given knowledge of $\mathbf{f}$, the resulting analog beams are denoted as $\mathbf{B}^{\text{est}} = [\mathbf{b}_1^{\text{est}}, \cdots, \mathbf{b}_{N_u}^{\text{est}}]$.

With the two analog beamforming schemes described above, we can assess the effectiveness of our proposed angular domain channel estimation by comparing the post-beamforming SINR. As a benchmark, we also calculate the maximum achievable SNR for each user using an *ideal beam* as defined in (31), assuming full channel knowledge and neglecting interference from other users. The performance is evaluated for three users, where each user's channel matrix consists of three clusters, each containing 10 equal-power paths. The cluster power levels are configured as follows: for user 1, all clusters have power P; for user 2, the clusters have power levels $P, 0.5P$, and $0.25P$; and for user 3, the clusters have power levels $P, 0.25P$ and $0.06P$. The power P is set so that, the average SINR per receive antenna for the three users, prior to beamforming, is about -13.5 dB, -15.9 dB, and -17.1 dB, respectively. After optimal beamforming, the SINR for the three users is approximately 9.8 dB, 7.5 dB, and 6.4 dB, respectively. The AoDs and AoAs for each cluster are uniformly generated, ensuring separations of $\vartheta_{M_V^\mathrm{r}}$ and $\vartheta_{M_H^\mathrm{r}}$ at the receiver. Within each cluster, the AoD/AoA paths are generated following the model described in Sec. IV. Cluster overlaps are permitted. We set $M_\mathrm{t} = 4 \times 4$ for each user and $M_\mathrm{r} = 16 \times 16$ for the AP. During the estimation process, we assume no prior knowledge of the number of clusters or paths. The algorithm begins by estimating the number of dominant paths and subsequently determines their parameters.

Fig. 10 presents the evaluations as the ratio of the SINR achieved to the SNR due to the ideal beam. The results for $N_d = 200$ are illustrated, with performance plotted across varying angular ranges. Evidently, *optimal beamformer* (OPT) performs close to the ideal case, even with interfering users, demonstrating the robustness and effectiveness of our proposed numerical solution. As angular spreads increase, the separation and power distribution of paths make angular-domain channel estimation more challenging. While the *estimation-based beamformer* (EST) shows a decrease in the SINR ratio as the angular spread widens, it still captures significant energy, particularly for small and moderate angular ranges. This suggests that the proposed algorithm with angular-domain estimation effectively separates individual users' signals onto their respective digital chains.

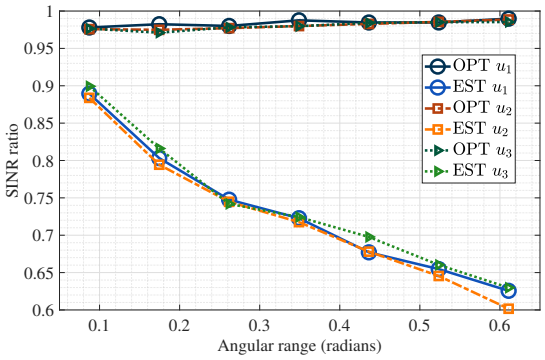

Fig. 10. SINR ratio vs. angular range for narrowband channels. $N_d = 200$.

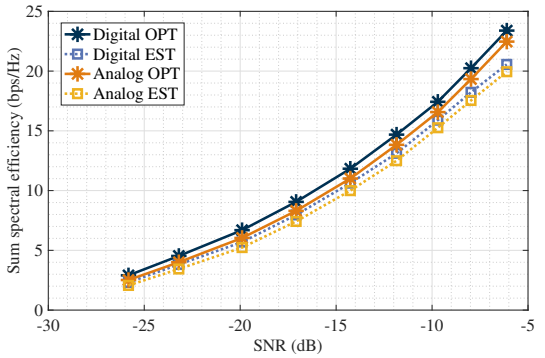

Fig. 11. Sum spectral efficiency vs. SINR of the weakest user.

We fix the angular range at 0.2618 radians and vary P to evaluate the sum spectral efficiency in different SNR settings. The results, shown in Fig. 11, depict the sum spectral efficiency as a function of the average SINR per receive antenna for the user with the weakest signal. Beyond analog beamforming, we extend our analysis to digital beamforming without the constant modulus constraint. The optimal digital beamformer is derived as $\mathbf{b}_u^0$, whose expression can be found in Sec. VI-A when we introduce *optimal beamformer*. We also derive the corresponding digital beamformer with AoA and gain estimates. To differentiate the digital beamformer and analog beamformer, they are denoted as Digital/Analog OPT for optimal digital/analog beamformer, and Digital/Analog EST for optimal digital/analog esimation-based beamformer, respectively. For the first two data points, $N_d = 480$. N_d is then halved every two data points untill reaching $N_d = 60$ for the last three data points. We then compare the sum spectral efficiency of all users across various beamforming schemes. Digital beamforming provides only marginal improvement over analog beamforming, whether using optimal or estimation-based approaches. This demonstrates the effectiveness of our proposed analog beamforming in enhancing users' SINR. Furthermore, our angular-domain estimation enables beamforming to achieve a sum spectral efficiency comparable

This article has been accepted for publication in IEEE Journal of Selected Topics in Signal Processing. This is the author's version which has not been fully edited and content may change prior to final publication. Citation information: DOI 10.1109/JSTSP.2025.3590607

to that obtained with perfect channel and transmit beamforming knowledge.

B. Beamforming for Wideband Channels

We begin by assessing the effectiveness of analog beamforming in reducing inter-user interference through the analysis of the post-beamforming SINR.

1) Wideband Optimal Beamformer: Without the constant modulus constraint, the optimal solution to problem (13) can be derived in closed form, denoted as $\mathbf{b}_u^0$. We then initialize the solution to (13) as $\angle\left(\mathbf{b}_u^0\right)$ and adopt a BCD-based algorithm to refine the phase components, with all ground-truth parameter values.

2) Wideband Estimation-Based Beamformer: When channel information is unknown, our goal is to reconstruct $\mathbf{H}_u[d]\mathbf{f}_u$, which can be expressed as

$$\mathbf{H}_u[d]\mathbf{f}_u = \sum_{l_u=1}^{L_u} \varsigma_{l_u} p(dT - \delta_{l_u}) \mathbf{a}_{M_\mathrm{r}}(\varphi_{l_u}, \theta_{l_u}). \tag{47}$$

We optimize over the parameters δ, φ, and θ for the $\widehat{L}_u$ dominant paths. Afterwards, we compute the ML estimate of ς_{l_u}. Following this, we proceed with the procedure described for *Wideband Optimal Beamformer* to determine the beamformer.

The simulations are based on the UMi fast fading channel model [42]. We simulate three users, where each user's channel matrix consists of four clusters, each containing 20 paths. We fix $M_\mathrm{r} = 8 \times 8$ at the AP, $M_\mathrm{t} = 4 \times 4$ for each user, and adopt $N_d = 200$. The heights of the user equipments are 1.75 m, 1.55 m, and 1.65 m, while the AP is 10 m. The AP is positioned at the origin, and a radiation range of π is defined to simulate signals from the front of the UPA at the AP. User 1 is located at an angle of 0.7728 radians, User 2 at 1.5674 radians, and User 3 at 2.5337 radians. We evaluate two scenarios: In the first scenario, users are placed at similar distances from the AP (d_0, $1.15d_0$, and $1.30d_0$), resulting in similar path loss and signal strengths. In the second scenario, users are positioned at varying distances (d_0', $1.5d_0'$, and $2d_0'$), leading to much more different signal strengths. The locations and heights of the user equipments remain fixed during the simulation, and path loss for each user is calculated to set the relative received power levels. Path propagation parameters, including delays and AoAs/AoDs, are independently and randomly generated in each realization. When multiple users transmit to the same AP, these parameters exhibit correlations, modeled as an exponential decay function with distance, as described in [48]. Despite the angular spreads defined in the UMi model, we adjust them to evaluate the robustness of our algorithm. We assume identical angular spreads for all AoAs and AoDs, representing them through angular ranges. Notably, under the given simulation settings, clusters may share similar AoAs/AoDs but differ in their delays. In the first setting, the average SINR per receive antenna before beamforming is approximately -10.8 dB, -13.1 dB, and -14.6 dB for users 1, 2, and 3, respectively. In the second setting, the average SINR is about -1.5 dB, -8.4 dB, and -12.6 dB, respectively. During the estimation,

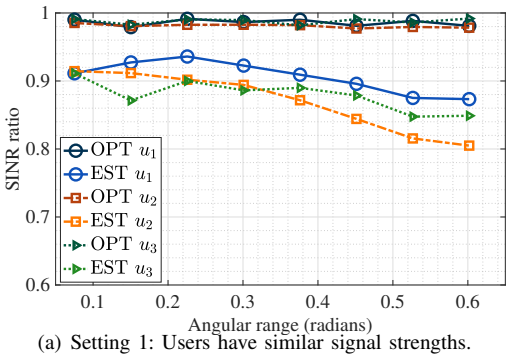

(a) Setting 1: Users have similar signal strengths.

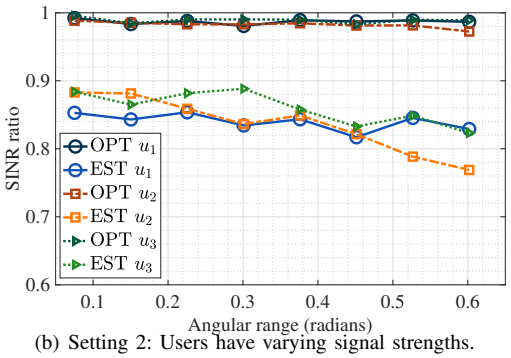

(b) Setting 2: Users have varying signal strengths.

Fig. 12. SINR ratio vs. angular range for wideband channels. $N_d = 200$.

we adopt $\widehat{L}_u = 4$ paths for all users. During communication, random BPSK symbols are transmitted to obtain the post-beamforming SINR. Similar results will be obtained for other constellations, as long as independence and power constraints are met. Simulation results are obtained by averaging over 200 independent random channel realizations, each spanning 1,000 symbol intervals during the communication phase.

Figure 12 illustrates the SINR ratio relative to the ideal scenario, which assumes full channel and transmit beamforming knowledge and no interference from other users. With *wideband optimal beamformers*, the SINRs for the three users are approximately 7.3, 5.0, and 3.7 dB, respectively, in Setting 1; and 17.3, 11.4, and 7.4 dB, respectively, in Setting 2. As shown in Fig. 12, with full channel and transmit beamforming knowledge, *wideband optimal beamformer* (OPT) achieves performance that closely approaches the ideal case. When users exhibit similar signal strengths, our proposed *wideband estimation-based beamformer* (EST) achieves SINR ratios of over 80% for all users across all tested angular ranges. With varying signal strengths, EST achieves SINR ratios of over 76% for all users across all angular ranges. Since user 2 is positioned between user 1 and user 3, its channel matrix exhibits the highest correlation with the other users, making it more susceptible to interference, particularly in Setting 1. As the angular range increases for user 2, channel estimation becomes more challenging, leading to a more pronounced decline in the SINR ratio. In contrast, the trend for the other users is less pronounced, especially when compared to the narrowband case. This can be attributed to the richer multipath propagation with delay spreads, where clusters can share angular similarities even with different delays. These similar AoAs enhances the effectiveness of our angular-domain-based

This article has been accepted for publication in IEEE Journal of Selected Topics in Signal Processing. This is the author's version which has not been fully edited and content may change prior to final publication. Citation information: DOI 10.1109/JSTSP.2025.3590607

beamforming computation.

C. Computational Complexity

In the narrowband multiuser case, the received measurements are first multiplied element-wise by each user's pilot sequence, incurring a complexity of $O(N_u M_{\mathrm{r}} N_d)$. Each user then performs angle and gain estimation following the single-user procedure, resulting in a total complexity of $O\left(N_u\left((M_V^{\mathrm{r}}+M_H^{\mathrm{r}}+I_{\mathrm{g}}\widehat{L})M_{\mathrm{r}}N_\zeta+M_{\mathrm{r}}N_d\right)\right)$.

In the wideband multiuser case, all users share the same exponent terms for likelihood computation, i.e., $\widetilde{\mu}_{i,m}^{\tau},\widetilde{\nu}_{i,m}^{\tau}$ for $h_u(\theta,\delta)$ and $\mu_m^{\tau},\nu_m^{\tau}$ for $\bar{h}_u(\varphi)$ (e.g., in Eq. (43)). Calculating these exponents incurs a one-time cost of $O(M_{\mathrm{r}}N_d)$. Each user u performs joint coarse sampling over elevation angles $\underline{\theta}_q$ (as defined in (23)) and delays $\delta\in\mathcal{D}$, where $|\mathcal{D}|=O(\varepsilon\widehat{D})$. With a selected δ, the computation of $\widetilde{\mathbf{s}}_u(\delta)$ costs $O(\widehat{D}N_d)$. Given $\widetilde{\mathbf{s}}_u(\delta)$ and precomputed exponents, the evaluation of $h_u(\theta,\delta)$ has a complexity of $O(M_{\mathrm{r}}N_dN_\zeta)$. Therefore, coarse sampling over all θ and δ combinations requires $O(M_V^{\mathrm{r}}\varepsilon\widehat{D}M_{\mathrm{r}}N_dN_\zeta)$. Refined elevation angle estimation is applied to $\widehat{L}_u$ selected coarse elevation angle estimates associated with their delay estimates using gradient descent, where each refinement involves I_{g} iterations. Thus, the elevation estimation cost becomes $O\left((M_V^{\mathrm{r}}\varepsilon\widehat{D}+I_{\mathrm{g}}\widehat{L}_u)M_{\mathrm{r}}N_dN_\zeta\right)$. For azimuth estimation, the delay estimates are utilized, and the cost of coarse sampling and refinement is $O\left((M_H^{\mathrm{r}}+I_{\mathrm{g}}\widehat{L}_u)M_{\mathrm{r}}N_dN_\zeta\right)$. With the final estimates $(\widehat{\theta}_u,\widehat{\varphi}_u)$ and $\widehat{\delta}_u$, each user estimates the effective path gain (amplitude and phase), requiring $O(M_{\mathrm{r}}N_d)$ per path. Hence, the total computational complexity across all users is: $O\left(M_{\mathrm{r}}N_d+N_u\left(\varepsilon\widehat{D}^2N_d+(M_V^{\mathrm{r}}\varepsilon\widehat{D}+M_H^{\mathrm{r}}+I_{\mathrm{g}}\widehat{L}_u)M_{\mathrm{r}}N_dN_\zeta\right)\right)$.

D. Equalization

With the analog beamforming, we can separate individual users' signals onto distinct digital chains, where the SINR of each user is maximized. However, due to varying path delays, inter-symbol interference remains on each digital chain. To address this, an equalization stage is introduced. We test for two different equalization schemes as outlined below. Afterwards, the equivalent E_b/N_0 (SNR per bit) is evaluated based on the achieved symbol error rate (SER). To facilitate SER-based analysis, the communication phase is set to span 10,000 symbol intervals, disregarding the coherence time constraint.

1) Adaptive Equalization: We employ the complex-valued recursive least squares algorithm to perform an adaptive equalization [49] for each user. To obtain the filter parameters, we introduce a training period with the hybrid architecture after applying the obtained analog beamformer. Let N_a denote the number of BPSK symbols used for adaptive training After a total training period comprising N_d+N_a symbols, we will have gained knowledge of both the analog beamforming and the equalization components.

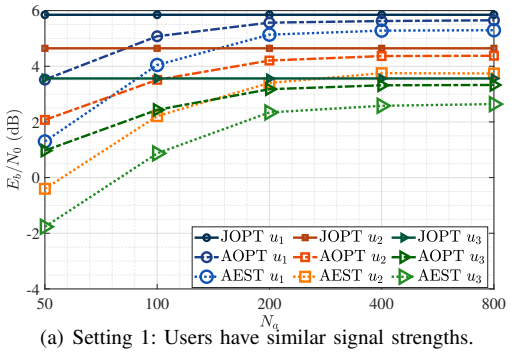

(a) Setting 1: Users have similar signal strengths.

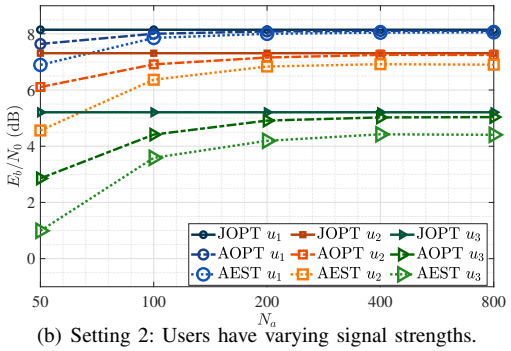

(b) Setting 2: Users have varying signal strengths.

Fig. 13. Equivalent SNR per bit after equalization vs. reference signal length for adaptive equalization. $N_d=200$.

2) Joint Equalization: Following analog beamforming, we apply equalization collectively to all users. We employ this scheme only when full channel knowledge is available. By leveraging full channel and transmit beamforming knowledge, it addresses both inter-user and inter-symbol interference in equalization design, serving as the upper bound for adaptive equalization performance. Specifically, we employ an MMSE decision feedback equalizer (DFE) as described in [50].

We adopt the same simulation settings as those for the post-beamforming SINR evaluation to assess the equalization performance following analog beamforming. The equivalent E_b/N_0 is plotted against N_a for adaptive equalization, as shown in Fig. 13. In the figure, joint equalization with full channel knowledge is labeled as JOPT, represented by a constant line since its performance is independent of N_a. We test with uncoded BPSK symbols, while higher-order constellations can be applied in scenarios with higher SNR. As N_a increases, the gap in the resulting E_b/N_0 between *wideband optimal beamformer* and *wideband estimation-based beamformer* reduces. For $N_a\geq 400$, adaptive equalization with *wideband estimation-based beamformer* (AEST) achieves a gap of within 0.36 dB for User 1, 0.64 dB for User 2, and 0.74 dB for User 3, compared to that with *wideband optimal beamformer* (AOPT) under setting 1. AEST achieves a gap of within 0.06 dB for User 1, 0.35 dB for User 2, and 0.63 dB for User 3, compared to AOPT under setting 2. This shows that our angular-domain channel estimation effectively supports *wideband estimation-based beamformer*, canceling the inter-user interference and enabling equalization to achieve performance close to that obtained with full channel and transmit beamforming knowledge, when the adaptive

training is sufficient. Additionally, the user with stronger signal strength experiences a smaller gap. In Setting 1, when users are positioned closer to each other, the increased interference and correlation between channel matrices lead to an overall larger gap, compared to Setting 2. We also observe that when users have similar power levels, joint equalization outperforms individual adaptive equalization by more effectively mitigating inter-user interference, but the performance gap between AEST and JOPT remains small when N_a is sufficiently large.

VII. Conclusion

We have proposed methods for angular-domain channel estimation and beamforming accelerated by full-dimension digital receive chains with 1-bit ADCs. The methods has been evaluated in narrowband and wideband channel scenarios in both single-user and multiuser systems, demonstrating robust performance across various conditions. In the narrowband case, the proposed analog beamforming effectively enhances users' SINRs, achieving sum spectral efficiency comparable to hybrid beamforming with perfect channel and transmit beamforming knowledge. In the wideband case, it enables signal equalization to further resolve inter-symbol interference, achieving SNR per bit performance close to the optimal scenario with perfect channel and transmit beam knowledge.

References

[1] H. Sheng, X. Chen, X. Zhai, A. Liu, and M.-J. Zhao, "Energy efficiency optimization for millimeter wave system with resolution-adaptive ADCs," *IEEE Wireless Commun. Lett.*, vol. 9, no. 9, pp. 1519–1523, 2020.

[2] D. Zhang, Y. Wang, X. Li, and W. Xiang, "Hybridly connected structure for hybrid beamforming in mmWave massive MIMO systems," *IEEE Trans. Commun.*, vol. 66, no. 2, pp. 662–674, 2017.

[3] L. Liu, W. Xiao, J. Liu, and Z. Rong, "Analog beamforming aided by full-dimension one-bit chains," in *Asilomar Conference on Signals, Systems, and Computers*. IEEE, 2024.

[4] W. B. Abbas, F. Gomez-Cuba, and M. Zorzi, "Millimeter wave receiver efficiency: A comprehensive comparison of beamforming schemes with low resolution ADCs," *IEEE Trans. Wireless Commun.*, vol. 16, no. 12, pp. 8131–8146, 2017.

[5] A. A. Nasir, H. D. Tuan, E. Dutkiewicz, and L. Hanzo, "Finite-resolution digital beamforming for multi-user millimeter-wave networks," *IEEE Trans. Veh. Technol.*, vol. 71, no. 9, pp. 9647–9662, 2022.

[6] L. Jiang and H. Jafarkhani, "Multi-user analog beamforming in millimeter wave MIMO systems based on path angle information," *IEEE Trans. Wireless Commun.*, vol. 18, no. 1, pp. 608–619, 2018.

[7] M. Zhu, T.-H. Chang, and M. Hong, "Learning to beamform in heterogeneous massive MIMO networks," *IEEE Trans. Wireless Commun.*, vol. 22, no. 7, pp. 4901–4915, 2022.

[8] O. El Ayach, S. Rajagopal, S. Abu-Surra, Z. Pi, and R. W. Heath, "Spatially sparse precoding in millimeter wave MIMO systems," *IEEE Trans. Wireless Commun.*, vol. 13, no. 3, pp. 1499–1513, 2014.

[9] Q. Shi and M. Hong, "Spectral efficiency optimization for millimeter wave multiuser MIMO systems," *IEEE J. Sel. Topics Signal Process.*, vol. 12, no. 3, pp. 455–468, 2018.

[10] J. A. Zhang, X. Huang, V. Dyadyuk, and Y. J. Guo, "Massive hybrid antenna array for millimeter-wave cellular communications," *IEEE Wireless Commun.*, vol. 22, no. 1, pp. 79–87, 2015.

[11] J. Zhang, W. Liu, C. Gu, S. S. Gao, and Q. Luo, "Robust multibeam multiplexing design based on a hybrid beamforming structure with nearly equal magnitude analogue coefficients," *IEEE Trans. Veh. Technol.*, vol. 71, no. 5, pp. 5564–5569, 2022.

[12] Q. Qin, L. Gui, P. Cheng, and B. Gong, "Time-varying channel estimation for millimeter wave multiuser MIMO systems," *IEEE Trans. Veh. Technol.*, vol. 67, no. 10, pp. 9435–9448, 2018.

[13] P. N. Alevizos, X. Fu, N. D. Sidiropoulos, Y. Yang, and A. Bletsas, "Limited feedback channel estimation in massive MIMO with non-uniform directional dictionaries," *IEEE Trans. Signal Process.*, vol. 66, no. 19, pp. 5127–5141, 2018.

[14] X. Cheng, C. Tang, and Z. Zhang, "Accurate channel estimation for millimeter-wave MIMO systems," *IEEE Trans. Veh. Technol.*, vol. 68, no. 5, pp. 5159–5163, 2019.

[15] P. Dong, H. Zhang, G. Y. Li, I. S. Gaspar, and N. NaderiAlizadeh, "Deep CNN-based channel estimation for mmWave massive MIMO systems," *IEEE J. Sel. Topics Signal Process.*, vol. 13, no. 5, pp. 989–1000, 2019.

[16] J. Gao, C. Zhong, G. Y. Li, J. B. Soriaga, and A. Behboodi, "Deep learning-based channel estimation for wideband hybrid mmWave massive MIMO," *IEEE Trans. Commun.*, vol. 71, no. 6, pp. 3679–3693, 2023.

[17] C.-K. Wen, C.-J. Wang, S. Jin, K.-K. Wong, and P. Ting, "Bayes-optimal joint channel-and-data estimation for massive MIMO with low-precision ADCs," *IEEE Trans. Signal Process.*, vol. 64, no. 10, pp. 2541–2556, 2015.

[18] J. Choi, J. Mo, and R. W. Heath, "Near maximum-likelihood detector and channel estimator for uplink multiuser massive MIMO systems with one-bit ADCs," *IEEE Trans. Commun.*, vol. 64, no. 5, pp. 2005–2018, 2016.

[19] Y. Li, C. Tao, G. Seco-Granados, A. Mezghani, A. L. Swindlehurst, and L. Liu, "Channel estimation and performance analysis of one-bit massive MIMO systems," *IEEE Trans. Signal Process.*, vol. 65, pp. 4075–4089, 2017.

[20] L. V. Nguyen, A. L. Swindlehurst, and D. H. Nguyen, "Svm-based channel estimation and data detection for one-bit massive MIMO systems," *IEEE Trans. Signal Process.*, vol. 69, pp. 2086–2099, 2021.

[21] Y. Dong, C. Chen, and Y. Jin, "AoAs and AoDs estimation for sparse millimeter wave channels with one-bit ADCs," in *International Conference on Wireless Communications & Signal Processing*. IEEE, 2016, pp. 1–5.

[22] J. Mo, P. Schniter, and R. W. Heath, "Channel estimation in broadband millimeter wave MIMO systems with few-bit ADCs," *IEEE Trans. Signal Process.*, vol. 66, pp. 1141–1154, 2018.

[23] L. Xu, C. Qian, F. Gao, W. Zhang, and S. Ma, "Angular domain channel estimation for mmWave massive MIMO with one-bit ADCs/DACs," *IEEE Trans. Wireless Commun.*, vol. 20, no. 2, pp. 969–982, 2020.

[24] Y. Wang, W. Xu, H. Zhang, and X. You, "Wideband mmWave channel estimation for hybrid massive MIMO with low-precision ADCs," *IEEE Wireless Commun. Lett.*, vol. 8, no. 1, pp. 285–288, 2018.

[25] R. Zhang, J. Zhang, Y. Gao, and H. Zhao, "Bussgang decomposition-based sparse channel estimation in wideband hybrid millimeter wave MIMO systems with finite-bit ADCs," *Digit. Signal Process.*, vol. 85, pp. 29–40, 2019.

[26] B. Srinivas, P. Priya, D. Sen, and S. Chakrabarti, "Channel estimation in sub-6 GHz and hybrid millimeter wave MIMO systems with low-resolution ADCs," *IEEE Trans. Green Commun. Netw.*, vol. PP, pp. 1–1, 2022.

[27] A. Mezghani and A. L. Swindlehurst, "Blind estimation of sparse broadband massive MIMO channels with ideal and one-bit ADCs," *IEEE Trans. Signal Process.*, vol. 66, pp. 2972–2983, 2018.

[28] F. Liu, H. Zhu, C. Li, J. Li, P. Wang, and P. V. Orlik, "Angular-domain channel estimation for one-bit massive MIMO systems: Performance bounds and algorithms," *IEEE Trans. Veh. Technol.*, vol. 69, no. 3, pp. 2928–2942, 2020.

[29] L. V. Nguyen, D. H. Nguyen, and A. L. Swindlehurst, "Deep learning for estimation and pilot signal design in few-bit massive MIMO systems," *IEEE Trans. Wireless Commun.*, vol. 22, no. 1, pp. 379–392, 2022.

[30] C. Qian, X. Fu, and N. D. Sidiropoulos, "Amplitude retrieval for channel estimation of MIMO systems with one-bit ADCs," *IEEE Signal Process. Lett.*, vol. 26, no. 11, pp. 1698–1702, 2019.

[31] M. Esfandiari, S. A. Vorobyov, and R. W. Heath, "Sparsity enforcing with Toeplitz matrix reconstruction method for mmWave UL channel estimation with one-bit ADCs," in *2022 IEEE 12th Sensor Array and Multichannel Signal Processing Workshop (SAM)*, 2022, pp. 141–145.

[32] ——, "ADMM-based solution for mmWave UL channel estimation with one-bit ADCs via sparsity enforcing and Toeplitz matrix reconstruction," in *IEEE International Conference on Communications*. IEEE, 2023, pp. 1338–1343.

[33] T. He and Z. Xiao, "Suboptimal beam search algorithm and codebook design for millimeter-wave communications," *Mobile Networks and Applications*, vol. 20, no. 1, pp. 86–97, 2015.

[34] Z. Xiao, T. He, P. Xia, and X.-G. Xia, "Hierarchical codebook design for beamforming training in millimeter-wave communication," *IEEE Trans. Wireless Commun.*, vol. 15, no. 5, pp. 3380–3392, 2016.

[35] A. Alkhateeb, O. El Ayach, G. Leus, and R. W. Heath, "Channel estimation and hybrid precoding for millimeter wave cellular systems," *IEEE J. Sel. Topics Signal Process.*, vol. 8, no. 5, pp. 831–846, 2014.
[36] R. Méndez-Rial, C. Rusu, N. González-Prelcic, A. Alkhateeb, and R. W. Heath, "Hybrid MIMO architectures for millimeter wave communications: Phase shifters or switches?" *IEEE access*, vol. 4, pp. 247–267, 2016.
[37] S.-H. Wu and G.-Y. Lu, "Compressive beam and channel tracking with reconfigurable hybrid beamforming in mmWave MIMO OFDM systems," *IEEE Trans. Wireless Commun.*, vol. 22, no. 2, pp. 1145–1160, 2022.
[38] G. Zhu, K. Huang, V. K. Lau, B. Xia, X. Li, and S. Zhang, "Hybrid beamforming via the kronecker decomposition for the millimeter-wave massive MIMO systems," *IEEE J. Sel. Areas Commun.*, vol. 35, no. 9, pp. 2097–2114, 2017.
[39] H. Huang, K. Liu, R. Wen, Y. Wang, and G. Wang, "Joint channel estimation and beamforming for millimeter wave cellular system," in *IEEE GLOBECOM*. IEEE, 2015, pp. 1–6.
[40] K. Kang, Q. Hu, Y. Cai, G. Yu, J. Hoydis, and Y. C. Eldar, "Joint channel estimation and hybrid beamforming via deep-unfolding," in *2022 30th European Signal Processing Conference (EUSIPCO)*. IEEE, 2022, pp. 658–662.
[41] M. A. Richards *et al.*, *Fundamentals of radar signal processing*. Mcgraw-hill New York, 2005, vol. 1.
[42] "3GPP TR 38.900 version 14.2.0 Release 14."
[43] Z. Xiao, H. Dong, L. Bai, P. Xia, and X.-G. Xia, "Enhanced channel estimation and codebook design for millimeter-wave communication," *IEEE Trans. Veh. Technol.*, vol. 67, no. 10, pp. 9393–9405, 2018.
[44] S. Rangan, "Generalized approximate message passing for estimation with random linear mixing," in *IEEE International Symposium on Information Theory Proceedings*. IEEE, 2011, pp. 2168–2172.
[45] S. Park, A. Alkhateeb, and R. W. Heath, "Dynamic subarrays for hybrid precoding in wideband mmWave MIMO systems," *IEEE Trans. Wireless Commun.*, vol. 16, no. 5, pp. 2907–2920, 2017.
[46] P. Manurkar, R. D. Horansky, B. F. Jamroz, J. A. Jargon, D. F. Williams, and K. A. Remley, "Precision millimeter-wave-modulated wideband source at 92.4 GHz as a step toward an over-the-air reference," *IEEE Trans. Microw. Theory Techn.*, vol. 68, no. 7, pp. 2644–2654, 2020.
[47] E. Björnson, E. Jorswieck *et al.*, "Optimal resource allocation in coordinated multi-cell systems," *Foundations and Trends® in Communications and Information Theory*, vol. 9, no. 2–3, pp. 113–381, 2013.
[48] W. II, "Winner II channel models," *IST-4-027756 WINNER II, D. 1. 1. 2 V1. 2*, 2007.
[49] P. S. Diniz *et al.*, *Adaptive filtering*. Springer, 1997, vol. 4.
[50] N. Al-Dhahir, "FIR channel-shortening equalizers for MIMO ISI channels," *IEEE Trans. Commun.*, vol. 49, no. 2, pp. 213–218, 2001.